journal of the mechanical behavior of biomedical materials 143 (2023) 105950

Contents lists available at ScienceDirect

Journal of the Mechanical Behavior of Biomedical Materials

journal homepage: www.elsevier.com/locate/jmbbm

Material extrusion of thermoplastic acrylic for intraoral devices: Technical feasibility and evaluation

Ankit Gupta [a], Frank Alifui-Segbaya [b,*], Seymur Hasanov [c], Alan R. White [d], Khaled E. Ahmed [b], Robert M. Love [b], Ismail Fidan [e,**]

[a] College of Engineering, Computer Science, and Technology, Department of Engineering and Technology, California State University, Los Angeles, USA
[b] School of Medicine and Dentistry, Ian O'Connor Building, Griffith Health, Gold Coast Campus, Griffith University, QLD, 4222, Australia
[c] Harvard John A. Paulson School of Engineering and Applied Sciences, Harvard University, Cambridge, MA, 02138, USA
[d] School of Environment and Science, Griffith Sciences, Nathan Campus, Griffith University, QLD, 4111, Australia
[e] Tennessee Tech University, 920 N. Peachtree Avenue, MET Department, LEWS 103, Cookeville, TN, 38505-5003, USA

ARTICLE INFO

Keywords:
Material extrusion
Polymethylmethacrylate
Denture base material
Fiber-reinforcement
Fiber-reinforced composites

ABSTRACT

With global demand for 3D printed medical devices on the rise, the search for safer, inexpensive, and sustainable methods is timely. Herein, we assessed the practicality of the material extrusion process for acrylic denture bases of which successful outcomes can be extended to implant surgical guides, orthodontic splints, impression trays, record bases and obturators for cleft palates or other maxillary defects. Representative materials comprising denture prototypes and test samples were designed and built with in-house polymethylmethacrylate filaments using varying print directions (PDs), layer heights (LHs) and reinforcements (RFs) with short glass fiber. The study undertook a comprehensive evaluation of the materials to determine their flexural, fracture, and thermal properties. Additional analyses for tensile and compressive properties, chemical composition, residual monomer, and surface roughness (Ra) were completed for parts with optimum parameters. Micrographic analysis of the acrylic composites revealed adequate fiber-matrix compatibility and predictably, their mechanical properties improved simultaneously with RFs and decreased LHs. Fiber reinforcement also improved the overall thermal conductivity of the materials. Ra, on the other hand, improved visibly with decreased RFs and LHs and the prototypes were effortlessly polished and characterized with veneering composites to mimic gingival tissues. In terms of chemical stability, the residual methyl methacrylate monomer contents are well below standards threshold for biological reactions. Notably, 5 vol% acrylic composites built with 0.05 mm LH in 0° on z-axis produced optimum properties that are superior to those of conventional acrylic, milled acrylic and 3D printed photopolymers. Finite element modeling successfully replicated the tensile properties of the prototypes. It may well be argued that the material extrusion process is cost-effective; however, the speed of manufacturing could be longer than that of established methods. Although the mean Ra is within an acceptable range, mandatory manual finishing and aesthetic pigmentation are required for long-term intraoral use. At a proof-of-concept level, it is evident that the material extrusion process can be applied to build inexpensive, safe, and robust thermoplastic acrylic devices. The broad outcomes of this novel study are equally worthy of academic reflection, and further translation to the clinic.

1. Introduction

Medical applications constitute one of the major breakthroughs of additive manufacturing for functional prototypes, personalized devices, and anatomical models (Ventola, 2014). In dentistry, the expanded implementation of the digital workflow especially in the last decade (van Noort, 2012) has accelerated the use of photopolymerization-based 3D printing (PB3DP) processes in place of subtractive manufacturing (computer numerical controlled milling) and conventional heat, chemical and light polymerization of acrylic or polymethylmethacrylate. In

* Corresponding author.
** Corresponding author.
E-mail addresses: agupta26@calstatela.edu (A. Gupta), f.alifui-segbaya@griffith.edu.au (F. Alifui-Segbaya), shasanov@seas.harvard.edu (S. Hasanov), alan.white@griffith.edu.au (A.R. White), khaled.ahmed@griffith.edu.au (K.E. Ahmed), r.love@griffith.edu.au (R.M. Love), ifidan@tntech.edu (I. Fidan).

https://doi.org/10.1016/j.jmbbm.2023.105950
Received 8 February 2023; Received in revised form 29 May 2023; Accepted 30 May 2023
Available online 2 June 2023

the context of convenience, vat-photopolymerization and material jetting techniques used in dental 3DP are comparatively fast as cross-linked polymers are speedily synthesized from multifunctional monomers and telechelic oligomers by photochemical reactions at ambient temperature (Alifui-Segbaya, 2020; Chua and Leong, 2015). Despite this, there are technical (Food and Drug Administration, 2016), processing (Stansbury and Idacavage, 2016; Bagheri and Jin, 2019), and safety constraints (Alifui-Segbaya et al., 2017, 2018, 2019a, 2020) that limit the general uptake of the various technologies and materials that must be determined on case-by-case basis. To this end, the utility of the material extrusion (ME) process could be explored not only as an alternative 3DP process but also for safer, cheaper, and sustainable manufacturing of devices for specialized applications in dentistry.

ME is a layer-based additive manufacturing process used to fabricate polymer or polymer composites by depositing a filament or bead of material from an extrusion head. Acrylic as a thermoplastic can be micro extruded at an elevated temperature and solidified on cooling. The extrusion process also allows the deposition of other classes of materials (e.g., thermosets, rubbers, polyurethanes, silicones, and functional polymers) (Nathan-Walleser et al., 2014) and solidification by different physical and chemical processes (Ligon et al., 2017). The benefits of multimaterial systems include lightweight, multi-coloured and hybrid modelling (Fidan et al., 2019; Hasanov et al., 2021), co-printing of temporary support materials for complex overhanging structures (Stansbury and Idacavage, 2016) and a potential development of well-fitting dentures with soft lining (to produce shock absorbing effect) for geriatric use or for patients with highly resorbed alveolar ridges and obturators for cleft palates or maxillary defects such as after tumour resection, as part of a digital workflow. Unlike PB3DP processes such as stereolithography and digital light processing, ME is a simple, stable (laser-free), and environmentally friendly process that relies on inexpensive hardware and software, process materials, reduced tooling, and postprocessing without direct exposure to harmful chemical compounds by users engaged in biomedically-related printing activities (Alifui--Segbaya et al., 2020).

With due cognizance of its limitations (Ligon et al., 2017; Dizon et al., 2018; Tran et al., 2022) and the little progress made thereof (Pieralli et al., 2020; Lüchtenborg et al., 2021), this study will attempt to utilize the ME process to construct acrylic denture base i.e., the part of a denture that rests on soft tissue, replaces lost soft tissue, offers lip support and retains the artificial teeth and evaluate its suitability for other applications such as implant surgical guides, orthodontic splints, impression trays, record bases and obturators for cleft palates.

2. Experimental

2.1. Filament production

The study commenced with in-house production of filaments using colourless polymethylmethacrylate (PMMA) pellets and additional short glass fiber (SGF) as a reinforcing material for polymer composite filaments. The production setup (Table 1) for filaments and representative parts is similar for pure and reinforced PMMAs (Fig. 1) without SGF in the former. The low-temperature furnace used to dry the constituents at 90 °C for 9h to prevent production defects from adsorbed moisture. The mixtures were poured into the hopper of the filament extruder and the single screw extruder was heated to allow the mixture to be extruded through a 1.75 mm hardened steel nozzle head as filaments. By adjusting the extruding parameters (265 °C temperature, 25 mm/s speed and 30 m/s air path speed), filament diameter ranging from 1.65 mm – 1.75 mm was accomplished.

Table 1
Physical and mechanical properties of raw polymethylmethacrylate and short glass fiber.

Properties	PMMA	SGF
Density (g/cm^3)	1.18	2.54
Glass transition temperature (°C)	105	-
Melting Point (°C)	265 – 285	>1000
Flexural Strength (MPa)	82 – 117	-
Flexural modulus (GPa)	2.4 – 3.4	-
Tensile strength (MPa)	55-75	2500 – 3450
Young's Modulus (GPa)	2.4 – 3.4	72.5

2.2. Prototyping and sampling

During part production stage, the Dremel 3D45 filament printer accessed the G-code before heating the 0.4 mm hardened steel nozzle head to melt the composite filament fed by a two-wheel drive. The head moved in the x-y plane on the build platform to print parts, bead by bead and then layer by layer. The build platform moved in the vertically downward direction (z plane) to allow the second layer to rest on the first layer.

The representative materials comprised pure (100%) PMMA and different reinforcements (RF) or fiber concentrations (FC): 97.5 vol% PMMA + 2.5 vol% SGF and 95 vol% PMMA + 5 vol% SGF. These were built in three print directions (PD) i.e., 0° in the z-axis, 90° in x-y plane, and 90° in z-axis) at 0.05, 0.1, 0.2 mm layer height (LH) of, on a platform set at 100 °C to prevent warping. Warpages were observed in the pilot samples probably due to residual stresses from the different thermal expansion and contraction of the materials. These were avoided when the parts were placed in an enclosed and controlled plexiglass chamber and allowed to cool down slowly. The chamber temperature was controlled, monitored, and maintained at 50 °C using a small heater and two probes. The enclosed chamber also helped in reducing material humidity and improving the layer-to-layer and fiber-matrix interfacial adhesion. Test batches were printed in three directions shown in Fig. 2, i.e., 0° in z-axis, 90° in x-y plane, and 90° in z-axis.

Test samples were designed, printed, and validated for standardized test methods before evaluated for fiber-matrix compatibility, flexural properties (strength and modulus), fracture properties (toughness and energy) and thermal properties (thermogravimetric analysis and conductivity). The dimensions of those tested for their flexural, tensile, and compressive properties are shown in Fig. 3. Additional data on tensile and compression properties, surface roughness, finite element analysis, chemical characterization and cost and build analysis are provided for materials built in 0° in z-axis being the ideal PD or print orientation for denture bases.

2.3. Microstructure analysis

The behavior of fiber length, concentration, distribution, and fiber-matrix interfacial adhesion considerably impacts the performance of composites (Gupta et al., 2020) hence it was necessary to investigate these variables before mechanical and thermal testing. PMMA/SGF samples (15 mm × 15 mm × 15 mm) were printed, polished, and analyzed using micrography. Additional potassium permanganate etching (sulfuric acid – 50 ml, orthophosphoric acid – 20 ml, distilled water – 5 ml, and potassium permanganate – 0.55 g) was performed to analyze fiber-matrix interfacial adhesion. The selective electron microscope (SEM) images (Fig. 4) of PMMA mixed with SGF (5 vol%) show surface morphology of uniformly distributed fibers in the PMMA matrixes. For this analysis, the gaps at the interface of fibers and the matrix are insignificant. The general assessment of the fiber-matrix behavior revealed (a) adequate compatibility, (b) uniform distribution for load transfer between materials, and (c) sufficient adhesion to enhance mechanical performance.

2.4. Flexural properties

Flexural strength and flexural modulus were measured for all materials. Under clinical conditions a denture material must withstand

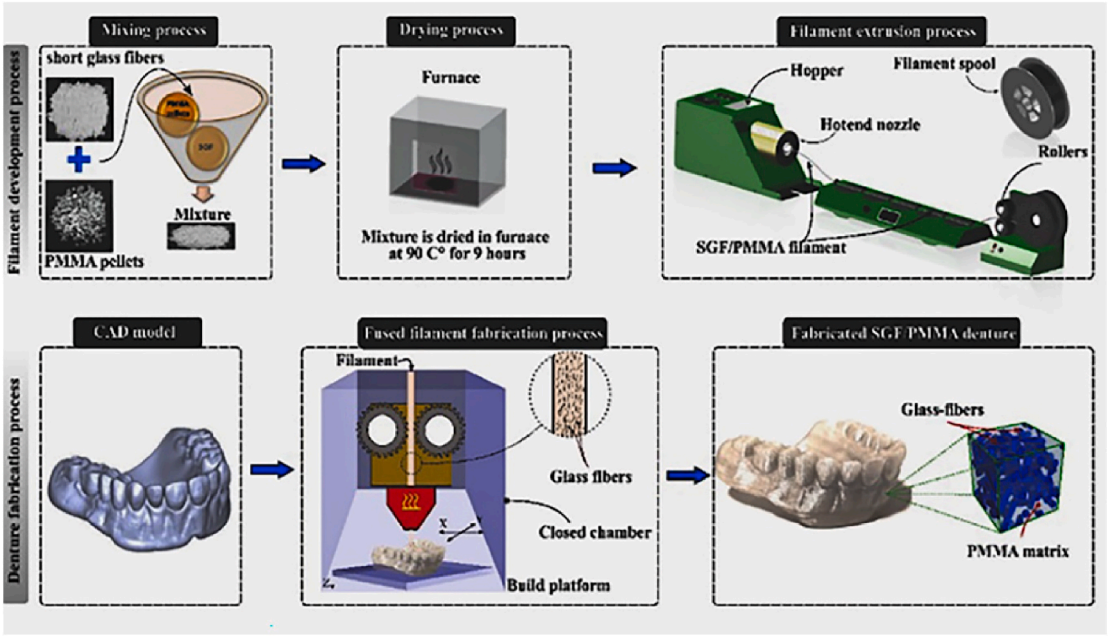

Fig. 1. Schematic of in-house filament and prototype production.

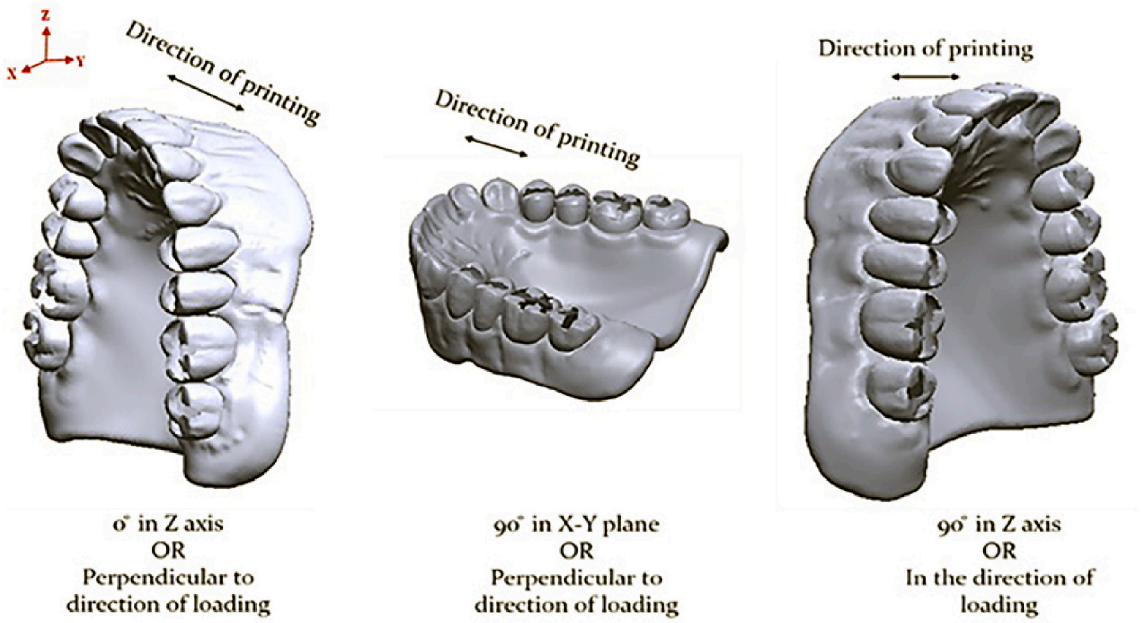

Fig. 2. 3D images of denture prototypes built with 0° in z-axis, 90° in x-y plane and 90° in z-axis print directions.

repeated flexing, bending, and withstand directed forces during mastication and speech, so a high flexural strength is desired. The flexural strength thus gauges the ability of a denture material to bend before it breaks. It is obtained when the ultimate flexibility of the material is achieved before its proportional limit (Mazumdar and Chowdhury, 2021). The flexural modulus, on the other hand, determines the material's stiffness or resistance to bending. This is calculated by measuring the slope of the linear portion of a typical stress-strain curve i.e., the change in stress divided by the corresponding change in strain.

2.4.1. Analysis of flexural strength and flexural modulus

The samples (n = 3) were tested in accordance with ISO 178:2019 (International Organization for Standardization, 2019). They were loaded in a three-point bending machine by precisely placing the sample perpendicular to the direction of load (Fig. 5). In a flexural test, stresses on the upper surface of the test samples tend to be compressive, whilst those on the lower surface are tensile (Fig. 6). Consequently, this test may be considered to combine elements of tensile and compressive testing (Fig. 7).

2.4.2. Effect of printing direction, layer height and fiber percentage on flexural properties

Due to the anisotropic nature of 3D printed parts, flexural testing was done in the PDs used for the samples; however, no plastic deformation and necking near the failure region was observed indicating brittle characteristics of the composite materials. Materials printed in 0° in z-axis with 0.05 mm LH, recorded the highest flexural strength and lowest flexural modulus (Fig. 8). Decreased LH created a good fusion between

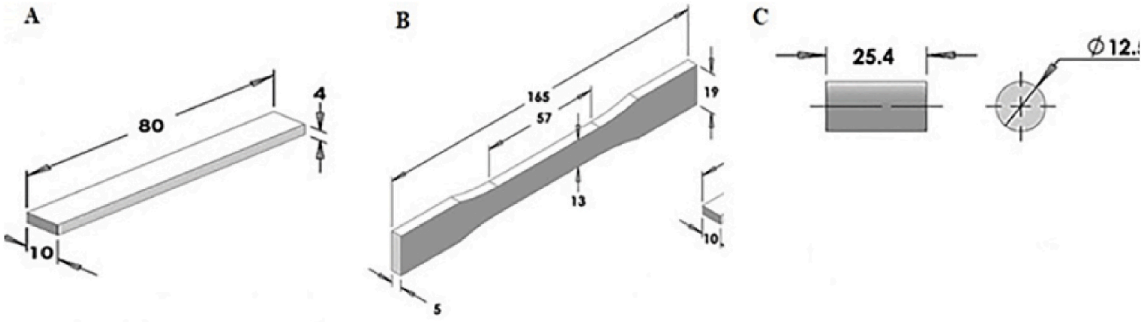

Fig. 3. Sample dimensions as per ASTM and ISO standards for (A) flexural, (B) tensile, and (C) compression testing of plastics.

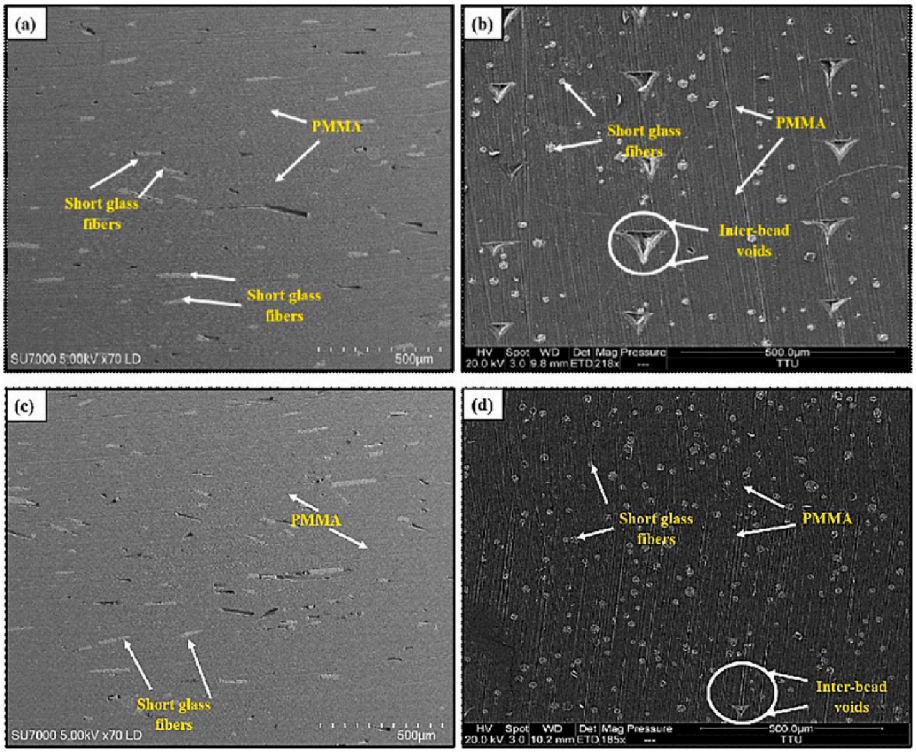

Fig. 4. Scanning electron microscope images of fiber (5 vol%) distribution in polymethylmethacrylate polymer matrix.

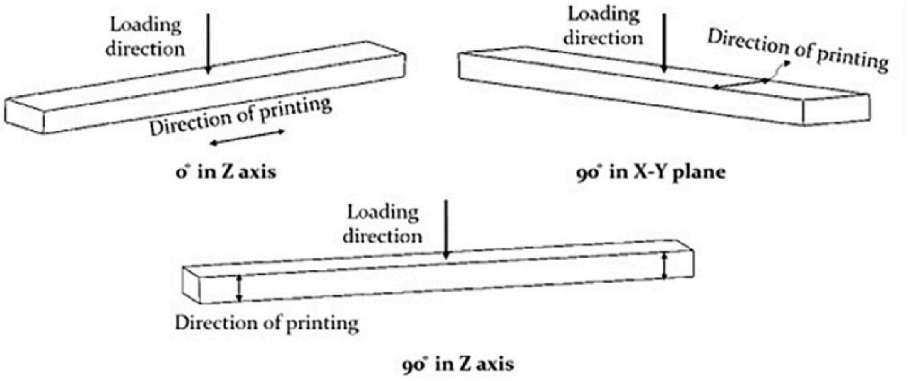

Fig. 5. Flexural samples with different printing directions and loading directions.

the adjacent layers which also helped to reduce the size of voids that are usually responsible for crack nucleation and propagation. The adhesion between the layers was also appropriate to deter the flow of crack and early fracture. Reinforcement (RF) proved effective in increasing flexural strength due to (a) good interfacial adhesion between the fibers and the matrix (b) more fiber loading leads to swelling of beads which

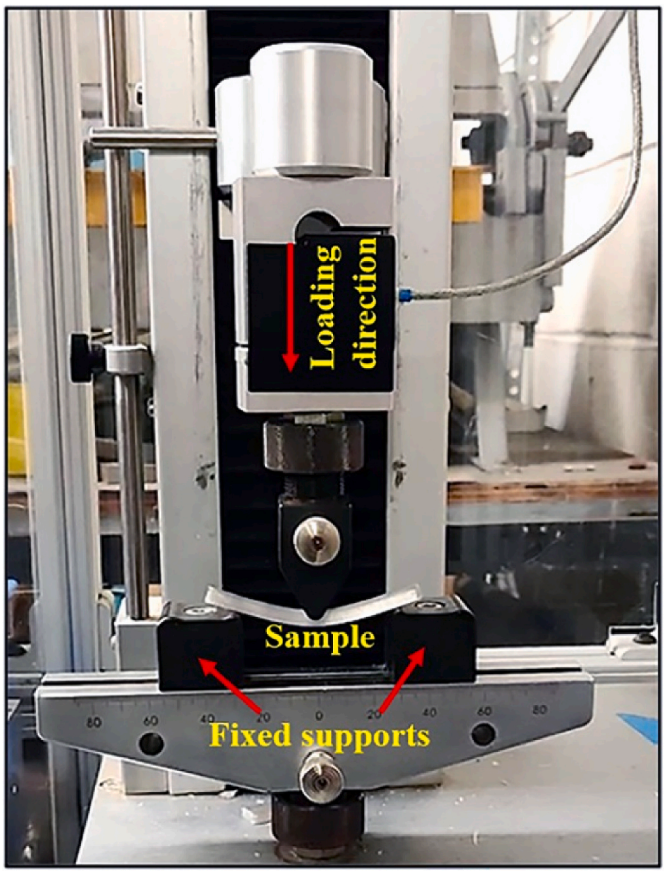

Fig. 6. Representative test specimen under tension and compression forces during flexural test.

decreases the void content and (c) hindrance created by fibers in the crack propagation. This may be due to strong mechanical interlocking between the layers and sufficient stress transfer from PMMA to SGF (Mazumdar and Chowdhury, 2021). The flexural strength was calculated from the load data using the following Eq. (1)

$$S = \frac{3PL}{2bd^2} \tag{1}$$

S – Flexural strength (MPa), P – maximum load before the fracture occurs (N), L – support span (mm), b – width of the specimen (mm), d – thickness of the specimen (mm). The strain in the samples was calculated using Eq. (2) by observing the change in the length of the sample.

$$e = \frac{6Dd}{L^2} \tag{2}$$

e – flexural strain in the outer surface (mm/mm), D – maximum deflection at the midspan (mm).

2.5. Fracture properties

Fracture properties measured the fracture toughness (FT) and fracture energy (FE) also known as strain energy release rate. FT as an essential mechanical property describes a material's ability to resist fracture (ability to absorb energy so that fracture is delayed) when it contains a crack. In context, it describes the resistance of a denture base material to propagation of flaws under an applied stress and assumes that the longer the flaw, the lower the stress needed to cause fracture. It is therefore proportional to the energy consumed in plastic deformation (Vaidya et al., 2019). FE, on the other hand, measures the elastic energy per unit area of crack growth (Sharafi et al., 2021) i.e., measurement of the energy to cause fracture. The fracture properties are clinically relevant, for instance, when dentures are dropped accidently or when patients are cleaning their dentures in a sink, or when the dentures have thin and weak spots in them due to the presence of irregular, protruding, underlying anatomy.

2.5.1. Fracture toughness analysis

The highly anisotropic nature of ME-produced parts creates significant constraints in investigating their fracture mechanics. FT thus depends on the material's loading type and mechanical behavior. During testing (ASTM D5045 (American Society for Testing and Materials International, 2013)) uniaxial load was applied at 0.1 mm/s to induce deformation in the sample (Fig. 9) before a complete rupture.

The initial crack length (a) also needed to be cut into the specimen, which was determined with the help of Eq. (3).

$$0 \cdot 45 < \frac{a}{W} < 0 \cdot 55 \tag{3}$$

The specimen was then loaded with the help of a 3-point bending machine by exactly placing the sample perpendicular to the direction of load. Fig. 11 (a) shows the direction of printing and direction of loading according to the ASTM – 5045. The FT was then calculated using Eq. (4).

$$K_{max} = \frac{fP_{max}l}{H \times W^{3/2}} \times \sqrt{10^{-3}}\ MPa\ m^{1/2} \tag{4}$$

Where, Pmax = maximum load exerted on the specimen (N).

H = Specimen thickness (mm), W = Specimen width (mm), a = initial crack length (mm), f(x) is the load calibration factor.

$$f(x) = \frac{6x^{1/2}[1.99 - x(1-x)(2.15 - 3.93x + 2.7x^2)]}{(1+2x) \times (1-x)^{3/2}} \tag{5}$$

$$x = \frac{a}{W} \tag{6}$$

2.5.2. Effect of printing direction, layer height and fiber percentage on fracture toughness

Equal load with feed rate was applied to all samples printed before failure occurred at ultimate strength. The failure surfaces of samples in 90° in z-axis were regular; however, irregularities were observed in samples in 0° in z-axis and 90° in x-y plane, indicating they might hinder crack propagation and increase FT (Fig. 10). Since unavoidable inter-bead voids i.e., crack nucleation sites when load is applied impact FT, those in 90° in z-axis loading direction encountered premature failure due to quick crack propagation. Lowering the LH provided a better fusion between the adjacent layers, decreased the voids, and increased the final fracture properties. The FT of the samples increased concurrently with fiber percentage due to hindrance created by fibers in the propagation of cracks. The increase is also due to reduced inter-bead void contents after reinforcing the fibers. The presence of fibers resulted in the swelling of each bead and ultimately reduced the void percentage (Gupta et al., 2022). Lowering the void size and its proportion in a printed material hindered the crack propagation and increased the FT.

2.5.3. Fracture energy analysis

FE or strain energy release rate measured elastic energy per unit area of crack growth (Sharafi et al., 2021). The fracture energy of the samples was calculated from the load-displacement curve using Eq. (7) and Eq. (8).

$$G_f = \frac{U\ (N\ mm)}{A\ (mm^2)} \tag{7}$$

U = area under the load versus load point deflection (LLPD) curve. It represents the energy required to break the specimen, A = Uncracked area at the notch (ligament area)

$$A = B\ (W - a_0) \tag{8}$$

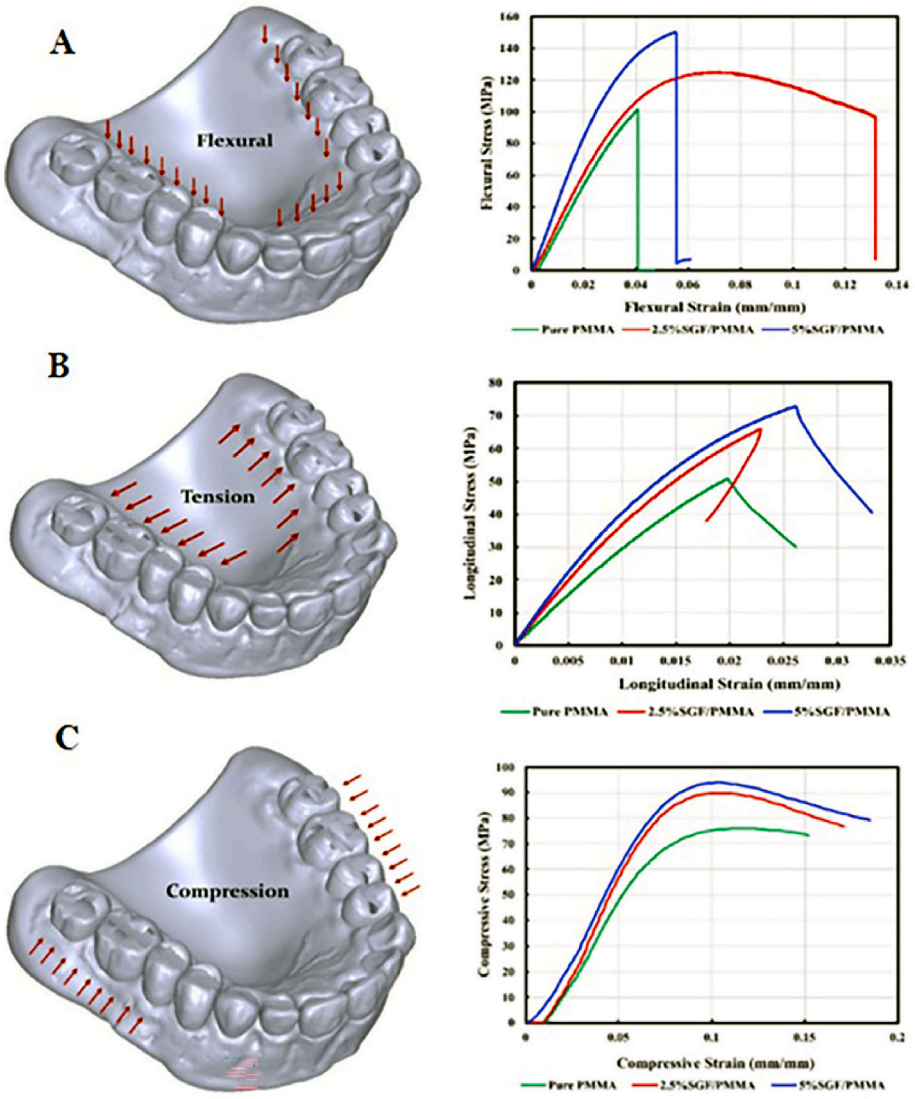

Fig. 7. Stress-strain curves of samples for flexural (A), tensile (B), and compressive (C) tests.

As in the case of FT, FE increased simultaneously with FC and decrease in LH (Fig. 11). It was also noticed that the FE is more for samples printed in 0° on the Z-axis (5.448 KJ/m2) as compared to samples printed in 90° in the x-y plane (1.853 KJ/m2), and 90° on z-axis (1.835 KJ/m2).

2.6. Fractography analysis

In this section, the surface morphology of fractured regions of samples (Fig. 12) used for fracture toughness and flexural tests are analyzed. The fractography analysis helped in investigating the PMMA/SGFs composite behavior under compression loading. Detailed SEM analysis was performed on the fractured area under high and low magnification as shown in Figs. 13 and 14.

The following were observed in the morphology of the fractured samples:

- Fibers are well distributed in the PMMA matrix without accumulation. The properties of SGFs hindered crack propagation and increased fracture toughness and flexural strength of the PMMA composites.
- Necking and plastic deformation were not observed in the failure region, an indication that the samples have brittle characteristics. This also justifies the good interfacial adhesion between the fibers and the matrix (Tian et al., 2016). Furthermore, it helped in reducing the fiber pull-out, matrix breakage, and aiding load transfer at the fiber-matrix interface. The general outcome is increased fracture toughness and flexural strength of samples printed in the three directions.

As discussed in the previous sections, there was substantial variation in the samples of the two properties in different PDs. Fracture behavior was the same for both fracture test and flexural samples. The samples with irregular crack propagation resulted in higher mechanical properties. Irregularities were higher in samples printed with 0° in the z-axis and 90° in the x-y plane in the case of FT samples. These were also higher for samples printed with 90° in the z-axis and 0° in the z-axis in the case of flexural samples. The irregularities in the crack propagation increased the fracture toughness of the samples. The crack direction was perpendicular to the fiber direction which may help in deflecting or stopping the crack propagation and could be another reason for the irregularities in the samples (Liu et al., 2018).

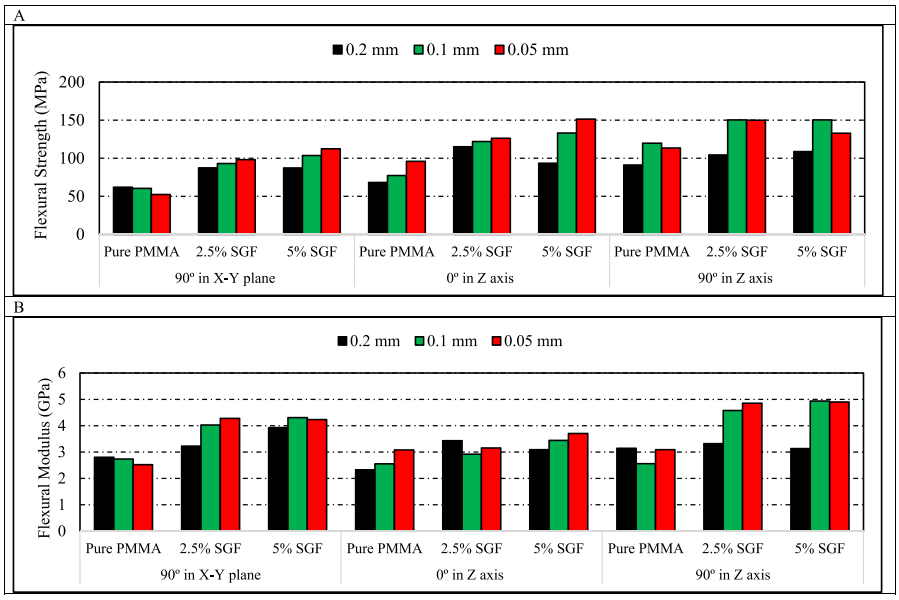

Fig. 8. Flexural strength (A) and flexural modulus (B) based on varying fiber reinforcement and layer heights of samples printed at 0° in z-axis, 90° in z-axis, and 90° in the x-y plane.

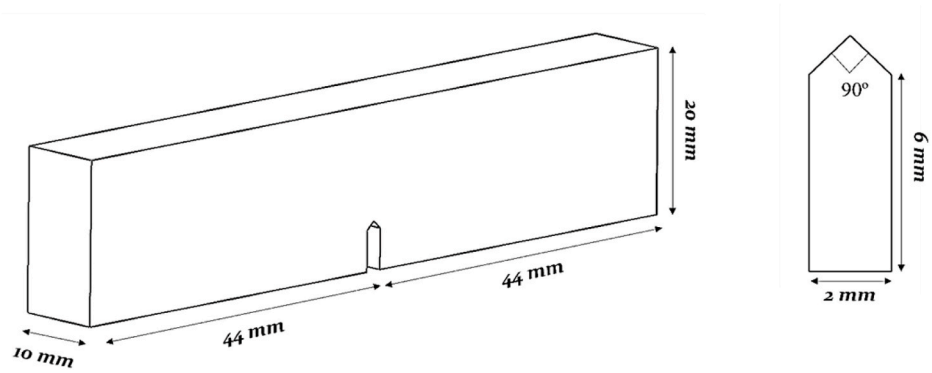

Fig. 9. Sample dimensions for ASTM D5045 fracture toughness test.

2.7. Thermal properties

The thermal properties measured are thermogravimetric analysis (TGA) and thermal conductivity analysis. TGA is used to determine a material's thermal stability and its fraction of volatile components by monitoring the weight change that occurs in a sample when it is heated at a constant rate (Rajisha et al., 2011). For acrylic composites it was performed to investigate its thermal stability by considering the change in weight with the change in temperature under a controlled nitrogen environment. Denture bases come in contact with mucosal surfaces so the transmission of a certain amount of thermal energy is desirable to convey the sensations of heat and cold from food and beverages. Thermal conductivity (κ) is a physical property that governs heat transfer through a material by conductive flow, increasing in the following order, although there are exceptions: polymers < ceramics < metals (Shen et al., 2022). Thermal conductivity analysis was performed to measure the impact of glass fiber on the increasing the thermal conductivity of the materials required for reducing sensation, better taste, and protecting intraoral tissues (Kul et al., 2016).

2.7.1. Thermogravimetric analysis

ASTM E1131 (American Society for Testing and Materials International, 2014) test guidelines were used to calculate the influence of glass fiber on the thermal degradation temperature of the acrylic composites. The analysis was performed using ceramic pans and heat was applied at the rate of 10 °C/min from room temperature to 800 °C in a controlled inert (nitrogen - in 60 ml/min) atmosphere. From room temperature (RT) to 150 °C, the weight loss mainly occurred due to moisture loss. The major weight loss occurred above 150 °C due to polymer degradation. It is evident in Fig. 15 and Table 2 that at 800 °C, the polymer degraded completely with some residues. The residue of 2.997 and 7.292 represents the presence of glass fibers in the case of PMMA/SGF (2.5 vol%) and PMMA/SGF (5 vol%) materials, respectively. The specimen's overall structure can be damaged by the early loss of glass fibers, which makes the residue calculation important. The results show that the glass fiber contents in the PMMA produced minimal effects on the thermal degradation or thermal stability hence the thermal insulation of the composites was mainly due to the insulating capacity of PMMA. The slight difference between the curves of pure PMMA and reinforced PMMAs is credited to the good dispersion of glass fibers in the PMMA.

2.7.2. Thermal conductivity analysis

Thermal conductivity (K) analysis was also performed in the three PDs due to the anisotropy using 50 mm x 20 mm x 20 mm samples with two 0.6 mm holes in the center (Fig. 16) and KD2 pro machine (KD2 Pro Thermal Properties Instrument (Wafer Sensor, Inc.) for measurement. two probes were carefully inserted in the holes. The setup was placed on a stale platform for 1h to attain an equilibrium temperature. Then

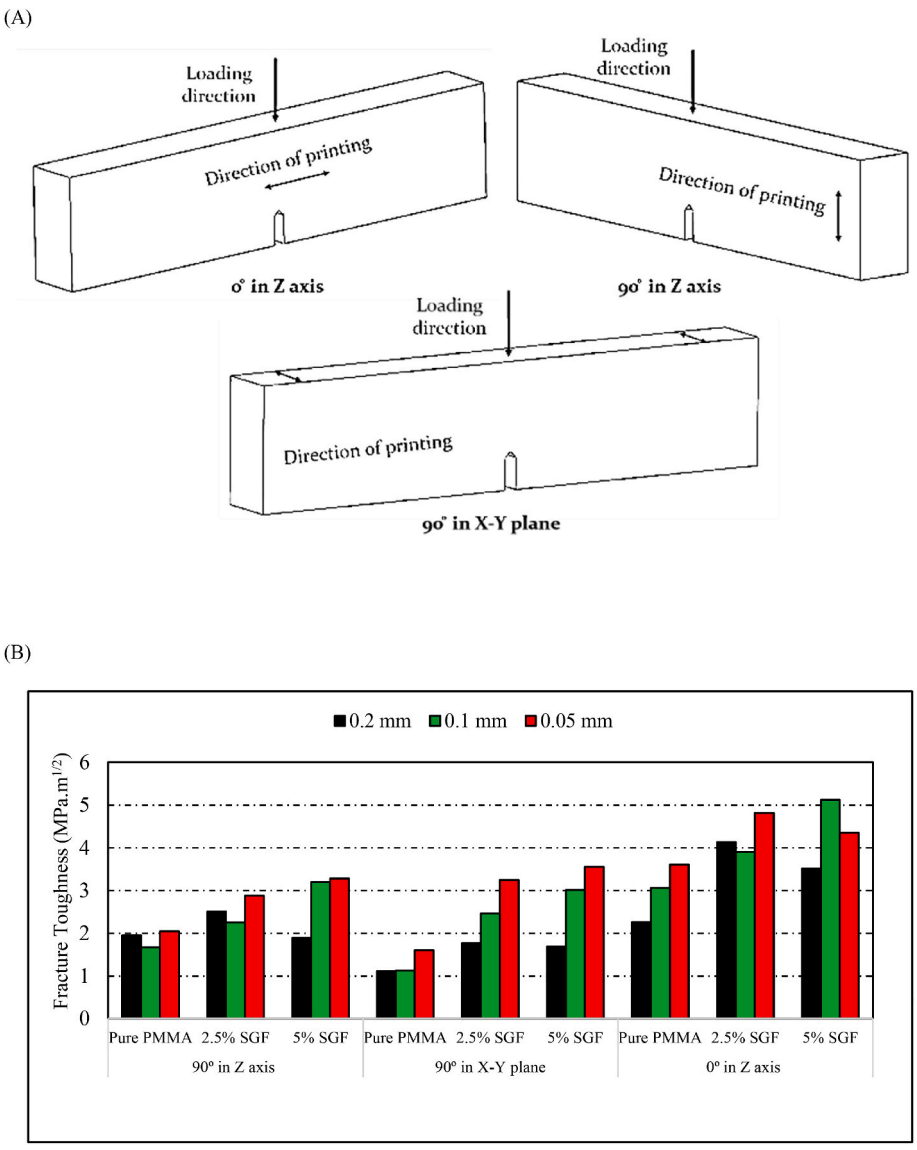

Fig. 10. Test samples with different print and loading directions for ASTM D 5045 during fracture toughness test (A) and fracture toughness data based on test parameters (B).

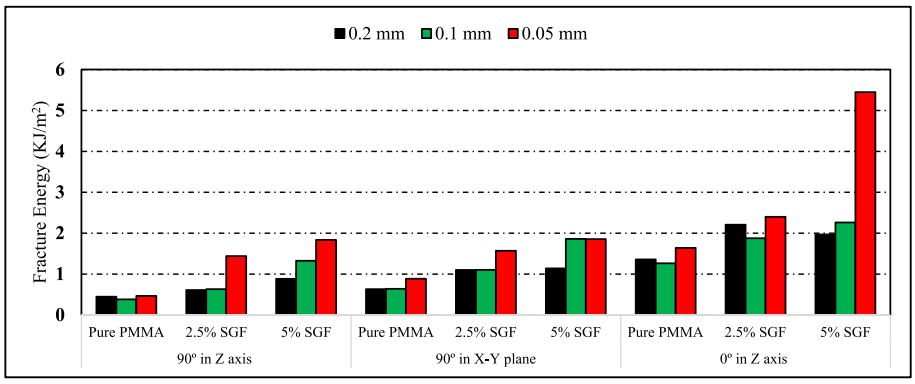

Fig. 11. Fracture energy of various fiber concentrations, layer heights and print directions.

temperature was increased to establish the temperature difference between the inner and outer surface. The tests were repeated three times for accuracy. K increased in samples printed at 90° in the x-y plane and 0° in the z-axis. Similarly, those with reinforced with glass fiber also displayed increased K (Fig. 17) due to interfacial thermal contact among the fibers.

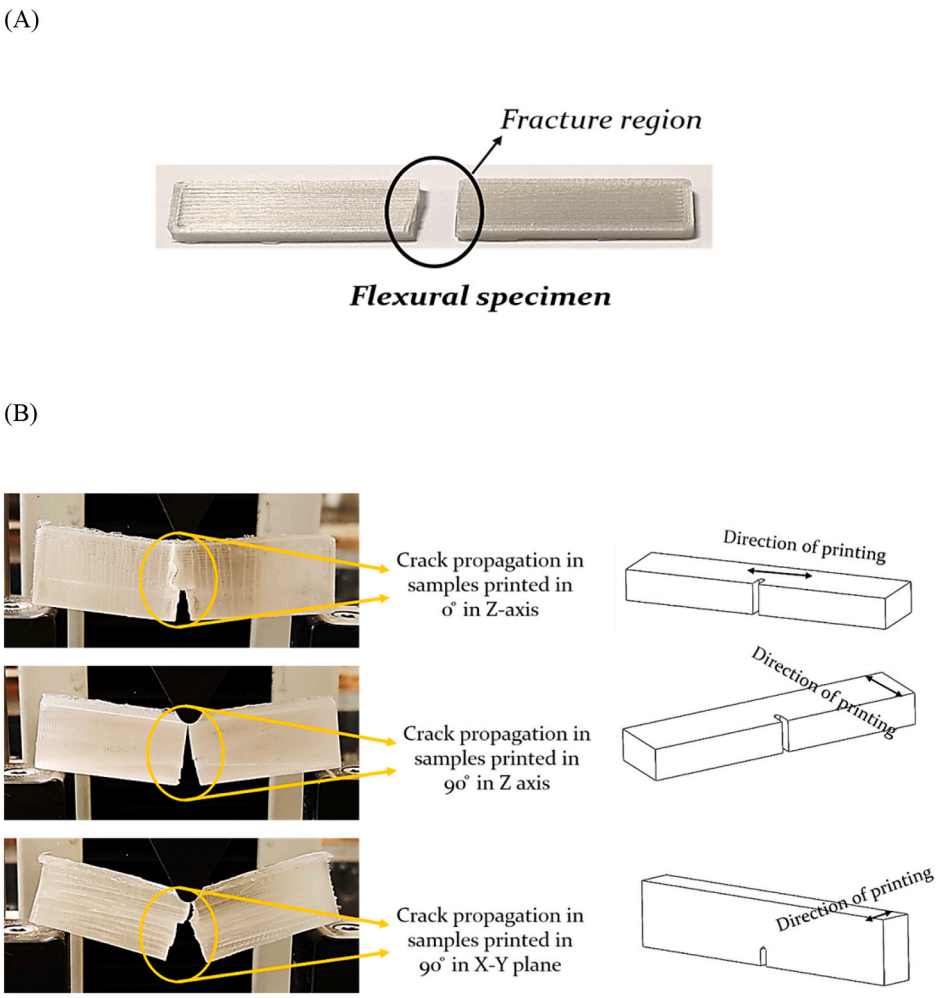

Fig. 12. Fractured samples after flexural(A) and fracture toughness (B) tests.

2.8. Tensile and compressive properties

2.8.1. Analysis for tensile properties

Tensile strength and tensile modulus of samples built in 0° in z-axis with different LHs were measured in accordance with ASTM D638 (American Society for Testing and Materials International, 2022). ASTM D638 standards measure of tensile strength is based on the amount of force that can be applied to the material before it yields or breaks. The tensile modulus determines how much the material can deform in response to stress before it yields (Lawrence, 2023). 3D printed dentures should have high tensile strength to prevent fractures and enhance stress transfer to denture bearing areas. The test samples (n = 5) were analyzed in ambient temperature with a strain rate and gauge length of 5 mm/min and 50 mm, respectively. Increased tensile properties (Fig. 18) were concurrent with fiber reinforcement and decreasing LHs due to adequate material compatibility, uniform fiber distribution in matrix, and uniform load transfer from fiber to matrix. Parts built with 0.05 mm LH showed the maximum improvement in tensile properties. As LH decreases, fusion in consecutive layers increases. Lowering LH also increases the number of layers in the fixed volume of tensile samples thus more layers will increase fusion and, a higher tensile strength.

2.8.2. Analysis for compressive properties

Compressive strength and compressive modulus of samples built in 0° in z-axis with different LHs were determined using test protocols in ASTM D695 (American Society for Testing and Materials International, 2016).The maximum of 2 KN load was applied on the cylindrical shaped samples at the rate of 0.05 inch/min. Only marginal increase in compressive properties (Fig. 19) were observed in majority of reinforced PMMAs. This may be due to the stress concentration at the fiber tip. The formation of stress at the tip could cause microcracks formations and propagation under the application of compressive load (Gupta et al., 2020). Slight changes in compressive strength and modulus were also noticed with the change in LH. This may be due to the direction of load application with LH.

2.9. Surface roughness

A major limitation of the ME technology is that surface roughness (Ra) or quality of “as-built” parts. To limit staircase effects commonly associated with the parts, the ideal process parameters were identified and used. Table 3 shows the input processing parameters used for denture base prototypes and test samples. Ra was also measured for test samples built in 0° in z-axis with the three LHs and fiber reinforcement. Infill density (100%), printing speed (30 mm/s), and extruder temperature (265 °C) are other dependent parameters.

Ra was measured using the Mitutoyo Ra profilometer with a stylus radius of 5 μm and a contact force of 4 mN. A measuring range of 10 mm (x-axis) and a linear speed of 0.25 mm/s was used for the testing. To avoid any warping during the relaxation period, enough adhesive was applied to the build platform. The sample was removed carefully from the build platform, and the measurements were taken using all four faces of the samples. A total of 5 readings were taken per face (Fig. 20) and an arithmetic mean Ra was used to express the final Ra value of the sample.

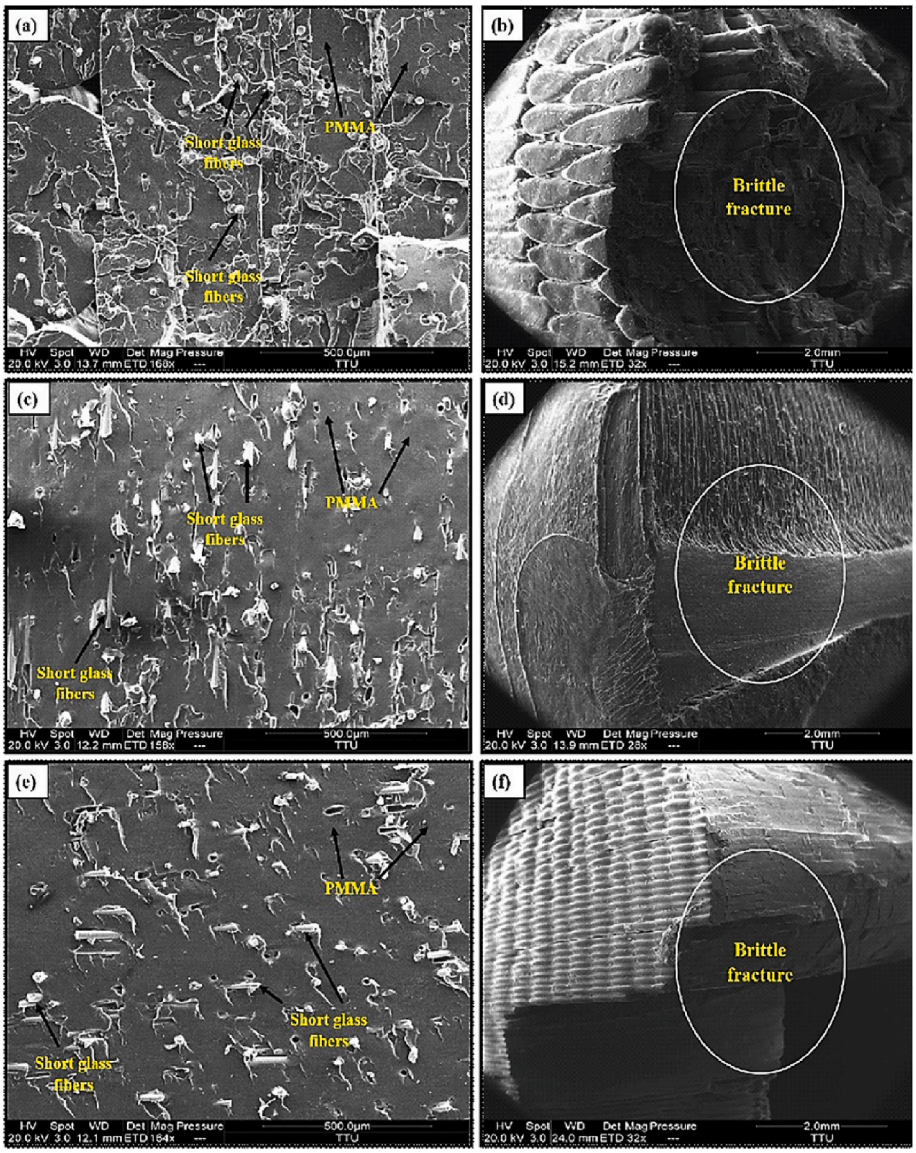

Fig. 13. SEM images of fractured surfaces observed in fracture toughness test samples printed in (a, b) 0° in z-axis, (c, d) 90° in z-axis, and (e, f) 90° in the x-y plane. Images are in low and high magnifications, respectively.

Table 4 shows the Ra values of all the faces, and the calculated mean and standard deviation values.

From the test results, RF and LH influenced the surface quality of the printed parts decreasing with increased RF/FC and LH (Fig. 21); however, the print time was much longer for samples with reduced LH. Table 5 shows the initial production cost, weight and build time of the prototypes. The materials cost for ME-produced reinforced methacrylate denture base is US$48/kg compared to ~ US$350/kg for a liquid resin used by 3DP techniques based on photopolymerization. The surface profile distribution (Fig. 22) shows variation in the Ra values with changes in RF (0 vol% vs. 5 vol%) and LH (0.05 mm, 0.1 mm and 0.2 mm) The Ra distributions for 0.05 mm LH samples have wider peaks-to-valleys than counterparts built with 0.2 mm LH; wider peaks-to-valleys were also observed for samples with higher RF.

2.10. Finite element analysis

Finite element (FE) analysis (Fig. 23) was performed to understand the predicted compressive behavior and stress concentration areas in the ME-produced PMMA dentures. Meshing was performed using the tetrahedron elements with a patch conforming algorithm. It is known that ME parts have anisotropy, especially, along the printing, transverse to the printing, and vertical printing directions. These properties are affected by the void areas inherited during the deposition process (Hasanov et al., 2021; Gupta et al., 2022). Therefore, the effective properties of the samples were computed using the numerical method called homogenization (Nasirov et al., 2020). Representative volume element (RVE) was taken from the microstructural descriptors, *e.g.*, microstructural images using the electron microscopy technique. User-defined RVE was incorporated into Material Designer (Ansys, Inc, USA, a computational software) to perform the material homogenization process. The details are provided in a previous work (Hasanov, 2021). Table 6 shows the homogenized properties of 3D printed PMMA materials. The error values shown in the table may be explained by the variety of factors such as complications created during the deposition process, the effect of print head vibrations, the moisture effect, microporosity, etc. (Hasanov et al., 2021). Effective properties agreed well with the experimental values that they can be used as input material data to simulate the denture base.

The stresses are concentrated where the compressive loads are applied and distributed over residual alveolar ridge area where the acrylic teeth are positioned. The information gathered from the FE

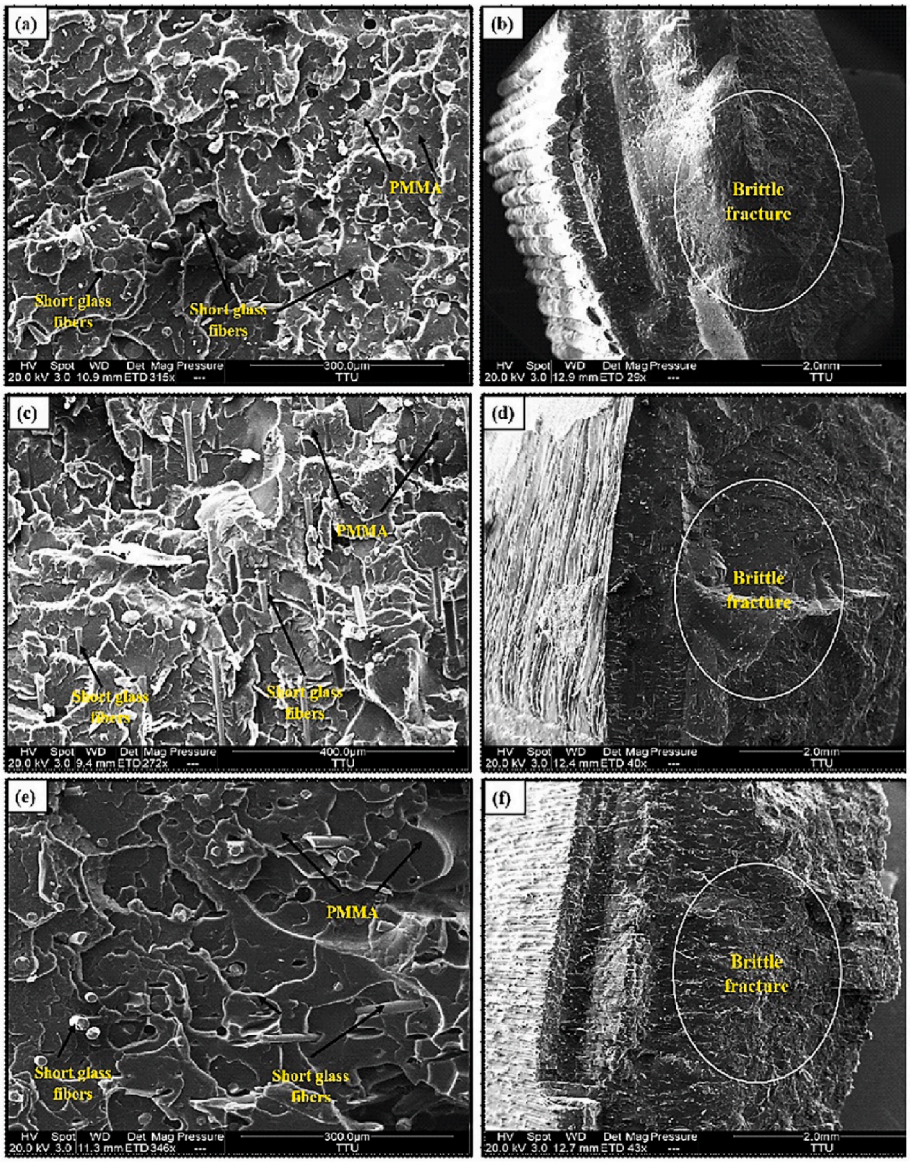

Fig. 14. SEM images of fractured surfaces observed in flexural test samples printed in (a, b) 0° in z-axis, (c, d) 90° in z-axis, and (e, f) 90° in the x-y plane. Images are in low and high magnifications, respectively.

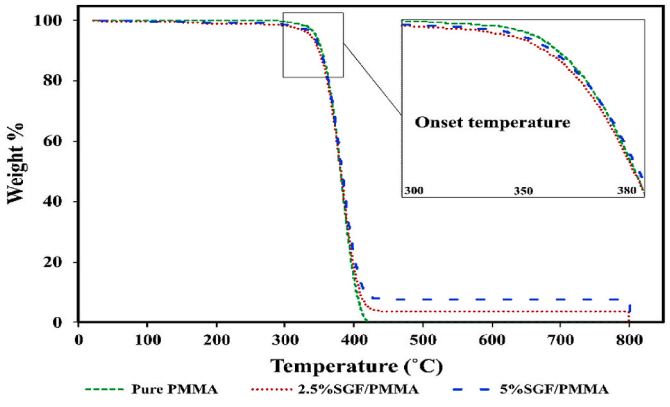

Fig. 15. Plot showing the thermal degradation of thermoplastic acrylic with different fiber concentration.

Table 2
Thermogravimetric analysis data showing material loss (%) with temperature increase.

Sample	RT – 150 (°C)	150 – 800 (°C)	Residue	T_{onset} (°C)
Pure PMMA	0.098	98.921	0.981	356.62
SCF/PMMA (2.5 vol%)	0.605	96.399	2.997	354.15
SCF/PMMA (5 vol%)	0.352	92.353	7.292	355.16

analysis will help to reinforce high stress concentration areas with glass fibers to obtain uniform stress distribution. Therefore, glass fibers will be incorporated where they are needed that will increase the product life cycle and reduce the material cost (Hasanov et al., 2022).

2.11. Chemical characterization

The PMMA samples (n = 3) were stored in a refrigerator at minus 20 °C to maintain their monomeric content before qualitative assessment for chemical compounds using headspace gas chromatography mass spectrometry (GCMS) (Alifui-Segbaya et al., 2020). For headspace

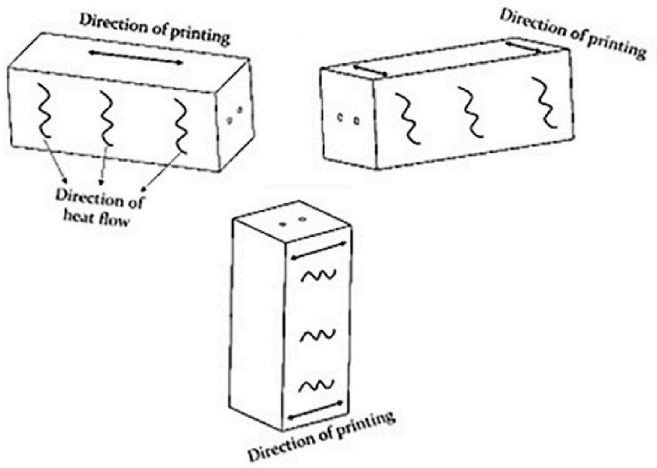

Fig. 16. Thermal conductivity samples with different printing directions and their respective direction of heat flow.

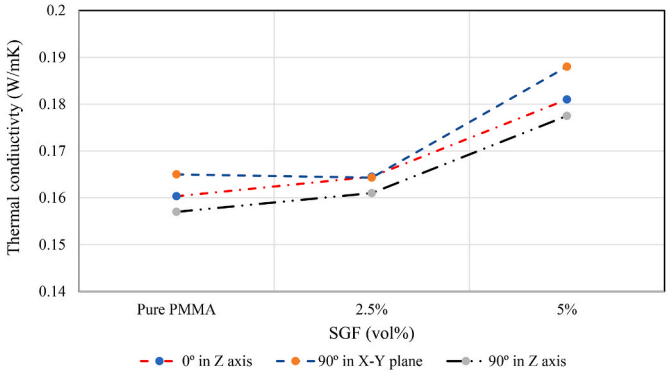

Fig. 17. Thermal conductivity performance of thermoplastic acrylic based on test parameters.

analysis, they were frozen in liquid nitrogen at -196 °C, pulverised, placed in a 20 ml vial and allowed to thermal equilibrate for 10 min. Sampling on a GC-Shimadzu TQ8040 GC–MS/MS (Shimadzu Corporation, Tokyo, Japan) involved extracting 1 ml aliquot of headspace gas and injecting onto a GC column (Agilent J&W DB5-MS 30 m 0.25 mm ID 0.25um film thickness). The test parameters used for headspace GC-MS were 40.0 °C column oven temperature, 250 °C injection temperature, 1.16 mL/min column flow rate, 5.0 split ratio and 15 min total run time. To ensure consistent measurements, the ambient air in the laboratory was analyzed as a "sample blank." This helped to establish the impurity level of each sample. Data were acquired via mass spectroscopy in a range of 41–600 m/z at an energy of 70 eV. The species were identified using NIST /EPA /NIH Mass Spectral Library 2014 (with >80% probability).

Table 7 shows the chemical compounds observed in pure and reinforced PMMA samples (n = 3), their molecular weight (MW) and retention time (RT). Of these, residual methyl methacrylate (MMA) monomer contents were quantified using gas chromatography with flame ionization detection (GCFID) in accordance with ISO 20795–1:2013 (International Organization for Standardization, 2013a) requirements for denture base materials. Standard solutions used for calibration yielded an r^2 value of 0.9989. Experiment was conducted in GC-2010plus (Shimadzu Corporation, Tokyo, Japan). The test parameters used were injection port temperature at 250 °C; FID detector temperature at 300 °C; initial temperature at 50 °C (2 min hold), 25 °C/min ramp to 75 °C (no hold), 150 °C/min ramp to 290 °C (hold 2.07 min) and 6.50 min total run time. Column gas flow rate, 1.37 mL/min. Split injection: 10:1. Restek Rxi-1MS column: 30.0 m length and 0.25 mm inner diameter. Residual MMA detected in unfiltered and filtered samples (n = 3) for pure and reinforced PMMA range between 0.43% and 0.47% mass fraction.

2.12. Statistical analysis

Statistical analysis was performed for SGF/PMMA materials. PD, FC, and LH (Table 8) are independent variables, whereas fracture toughness, flexural strength, flexural modulus (1.9 MPa $m^{1/2}$, 65 MPa, 2 GPa respectively)), fracture energy (0.9 kJ/m^2), and thermal conductivity constitute the dependent variables. Only the fracture toughness is analyzed here as an additional requirements for materials with improved impact resistance on the basis that the SGF/PMMAs tested meets standards requirements to be considered as materials with improved impact resistance with the maximum stress intensity factor is more 1.9 MPa $m^{1/2}$ (ISO, 20795-1) (International Organization for Standardization, 2013a).

2.12.1. Data validation

Residual vs. predicted plot and residual normal quantile plot were also plotted in this case to investigate the normal distribution of the residuals. Fig. 24 (a, c) show that the points are close to the diagonal line, which indicates the high R-square value (FT - 0.915975, FE - 0.813372) of the model. The error variance is constant across various levels of the dependent variables. The model seems to provide a good fit. Fig. 24 (b, d) also shows that the errors are normally distributed. So, residuals are approximately normally distributed.

2.12.2. Residual analysis

Residual analysis verified the conditions for drawing inferences about the coefficients in a linear model. For a valid linear mode, the residuals will:

- have a constant variance
- be approximately normally distributed (with a mean of zero), and

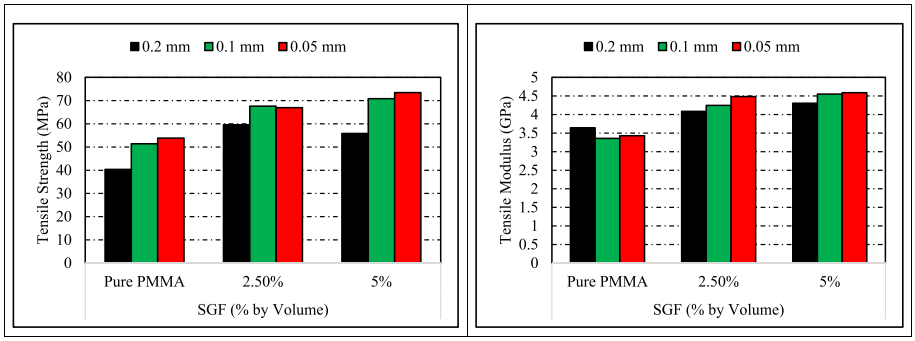

Fig. 18. Tensile strength and tensile modulus of samples built in 0° in z-axis and evaluated in accordance with ASTM D638.

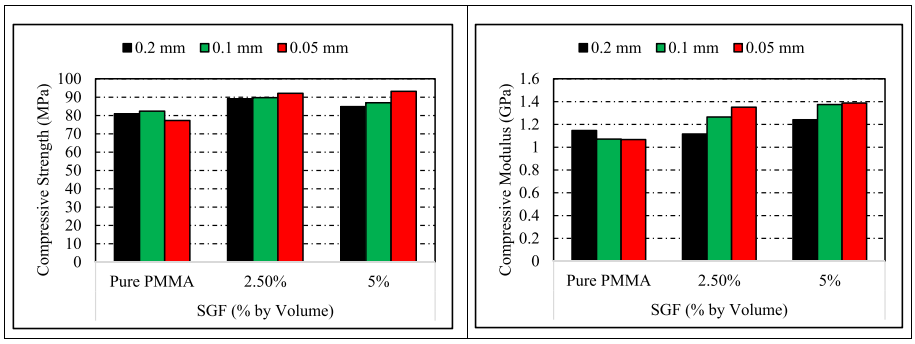

Fig. 19. Compressive strength and compressive modulus of samples built in 0° in z-axis and evaluated in accordance with ASTM D695.

Table 3
Build parameters for test samples and prototypes.

Properties	Values
Layer height (mm)	0.2, 0.1, 0.05
Layer width (mm)	0.35
Infill line width (mm)	0.4
Extrusion temperature (°C)	265
Infill density (%)	100
Infill pattern	Line
Shells	1
Top layers	0
Bottom layers	0
Infill overlap (mm)	0
Flow (%)	100
Printing speed (mm/sec)	30
Travel speed (mm/sec)	30
Room temperature (°C)	25 - 27
Humidity (%)	35 - 40

- be independent of one another over time

An observation is considered an outlier relative to other response values if it is extreme. Studentized residuals falling outside the red limits are potential outliers. Fig. 25 shows that the studentized residuals are not falling outside the red limits, so there are no outliers or unusual observations in this model. This confirms the equality of the variance.

2.12.3. Analysis of variance (ANOVA)

ANOVA analysis was performed to investigate the influence of individual parameters and their interactions on the FT and FE results. The ANOVA model chosen is shown in Eq. (9) (Barnett, 1975).

$$Y_{ijk} = \mu.. + \alpha_i + \beta_j + \gamma_k + (\alpha\beta)_{ij} + (\beta\gamma)_{jk} + (\gamma\alpha)_{ik} + (\alpha\beta\gamma)_{ijk} + \varepsilon_{ijk} \quad (9)$$

$\mu..$ is a constant (overall mean), α_i is the main effect for factor A (print direction) at the ith level, β_j is the main effect for factor B (FC) at the jth level, γ_k is the main effect for factor C (layer height) at the level, $(\alpha\beta)_{ij}$, $(\beta\gamma)_{jk}$, $(\beta\gamma)_{jk}$, and $(\alpha\beta\gamma)_{ijk}$ are the interaction effects. Table 9 shows the ANOVA for FT and FE and their interaction: build direction, fiber reinforcement, and LH have a p-value less than 0.05 making them significant factors. The two-way interaction of orientation with reinforcement concentration with LH is insignificant. But two-way interaction of concentration with LH shows a significant impact. The ANOVA confirmed that PD, LH, RF, and two-way interaction of concentration with LH significantly influenced FT and FE.

Key: DOF - degree of freedom.

3. Discussion

In 3DP, acrylic or PMMA is widely used as an engineering material. As a thermoplastic polymer, it must be softened by heating it slightly above its melting point, extruded, deposited, and solidified on cooling. In ME, the inherent process limitations and material properties are known to cause mechanical property deficiency and related anisotropy with respect to build direction of the printed parts (Väyrynen et al., 2016). Studies have identified raster orientation, LH, layer thickness, extruder temperature, feed rate, gap between raster, and build orientation as critical parameters that could potentially affect mechanical

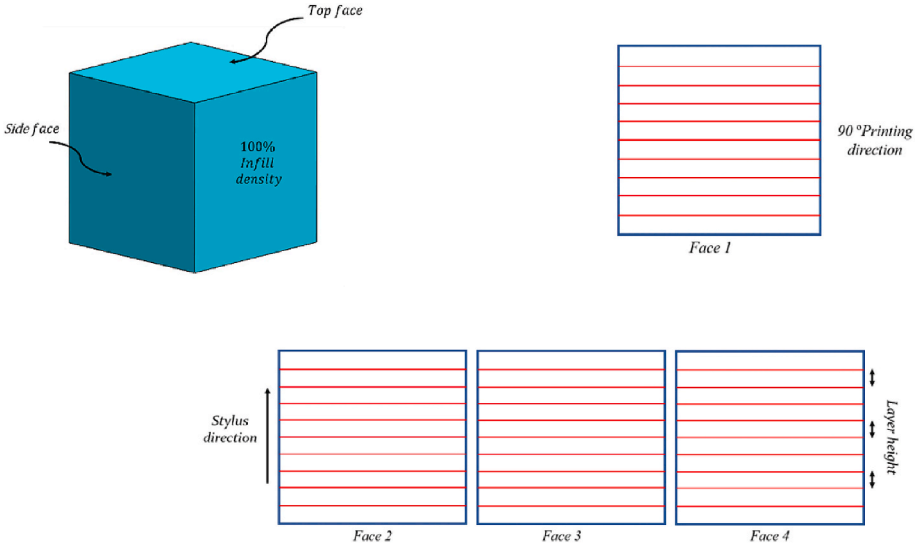

Fig. 20. Sample faces with printing direction and measuring direction for surface roughness analysis.

Table 4
Surface roughness data based on different faces of composite samples.

		Face 1 (μm)	Face 2 (μm)	Face 3 (μm)	Face 4 (μm)	Mean (μm)	SD (μm)
Pure PMMA	0.2	15.338	14.26	16.2468	15.561	15.3514	0.824
	0.1	9.4796	9.6522	9.7176	8.046	9.2238	0.7916
	0.05	4.339	4.6738	7.979	5.7406	5.6831	1.6431
2.5 vol% PMMA/SGF	0.2	16.0558	15.5448	17.1284	15.1358	15.9662	0.8614
	0.1	9.7024	10.6522	8.3678	9.5394	9.5655	0.9372
	0.05	6.7514	7.414	6.9068	5.6386	6.6777	0.7483
5 vol% PMMA/SGF	0.2	17.0316	17.6854	17.8458	19.8266	18.0973	1.2054
	0.1	8.9464	9.5488	10.7046	9.9148	9.7786	0.7352
	0.05	8.4744	9.8626	9.5936	7.9898	8.9801	0.8929

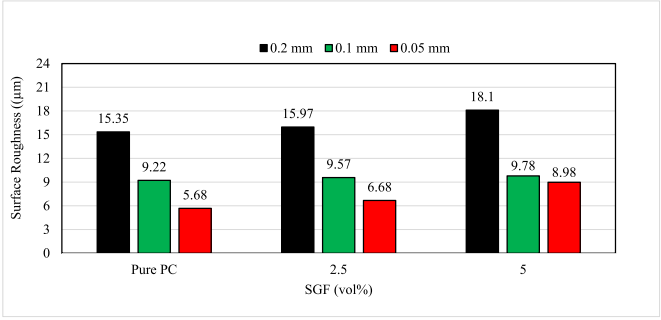

Fig. 21. Surface roughness values for different fiber concentrations and layer heights.

Table 5
Comparison of initial production cost, weight and build time of denture base prototypes.

Product			Cost (US$)
Acrylic/PMMA pellets			25$/Kg
Short glass fiber			23$/Kg
Denture base (PMMA)			0.575$/23g
Denture base (2.5 vol% PMMA/SGF)			0.5726$/23g
Denture base (5 vol% PMMA/SGF)			0.5705$/23g
Sample	**Layer height (mm)**	**Weight (g)**	**Manufacturing time (h)**
Denture Base (Pure PMMA)	0.2	20.72	3.3 h
Denture Base (Pure PMMA)	0.1	21.28	6.6 h
Denture Base (Pure PMMA)	0.05	21.09	9.9 h
Denture base (2.5 vol% PMMA/SGF)	0.2	17.63	3.3 h
Denture base (2.5 vol% PMMA/SGF)	0.1	18.82	6.6 h
Denture base (5 vol% PMMA/SGF)	0.2	19.66	3.3 h

properties and fatigue life of ME-produced parts (Terekhina et al., 2020). In this study, relevant parameters were identified and applied at the pilot stage. Optimum properties were obtained for parts built with 5 vol% RF, 0.05 mm LH and 0° in z-axis PD. It is worth stating that 0° in z-axis orientation guaranteed superior quality print without support structures on the fitting surface of the prototypes. The SGF limit in the matrix ensured ease of processing. Similarly, 50 °C enclosed chamber prevented warpage and electronic malfunction of the hardware. These together with the build parameters guaranteed satisfactory test samples and prototypes for evaluation.

The reference data in Table 10 compares the physico-mechanical properties of the best performing PMMA materials with standards requirements (International Organization for Standardization, 2013a) for acrylic denture base material. By combining PMMA (matrix) and short glass fiber (reinforcing material), the resultant polymer composites presented improved properties that are not achievable with one material (Vaidya et al., 2019). The requirements of a denture base material used in dentistry fall mostly under physical, mechanical, chemical, thermal, aesthetic, and biological properties. Other relevant requirements include ease of processing, repair, and affordability (Nejatian et al., 2019; Sideridou, 2010). The reinforced PMMA exhibited high strength, thermal conductivity, durability, and modulus of elasticity compared to raw and pure PMMA. These together with established PMMA properties (lightweight, aesthetics, low water sorption and solubility, ease of processing and repair) will guarantee superior performance (Sakaguchi and Powers, 2012).

In this study, the FT and FE of PMMA also increased concurrently with FC (vol%). It is noteworthy that the inherently low FT of conventional acrylic denture base materials has also been improved with short glass, carbon, and Kevlar-reinforcement. Likewise, the bulk contribution to the overall FE has been linked to the energy associated with fiber fracture. This occurs when the fiber is stretched during the crack tip opening, sliding against the matrix, and after breakage retracts into the matrix releasing its stored elastic energy (Jancar et al., 2009). A notable increase in tensile properties was reported for 5 vol% hybrid reinforcement of denture base resin with glass fibers and zirconium oxide nanoparticles (Gad et al., 2018). Researchers have also recommended the use of glass fibers and aramid for increasing the flexural strength of PMMA (John et al., 2001). A recent review identified flexural strength as the most studied mechanical property of 3D printed denture base material ahead of impact resistance, hardness, elastic modulus, and fracture toughness (Lourinho et al., 2022). A study that compared the flexural strength, hardness, and surface roughness of heat-polymerized acrylic (A) versus 3D-printed denture base photopolymer (B) reported the following: flexural strength (MPa) 86.63 ± 1.0 (A) and 69.15 ± 0.88 (B), impact strength (KJ/m^2) 6.32 ± 0.50 (A) and 2.44 ± 0.31 (B), hardness (VHN) 41.63 ± 2.03 (A) and 34.62 ± 2.1 (B), and surface roughness (μm) -0.18 ± 0.01(A) and 0.12 ± 0.02 (B) (Gad et al., 2022). Within the conventional denture base group, a study compared the flexural strength and modulus of light and heat-cured urethane dimethacrylate (C), heat cured acrylic (D) and auto-polymerized acrylic (E). The flexural strengths (MPa) reported are 103 ± 4 (C), 78 ± 3 (D), and 63 ± 4 (E) and the flexural moduli (MPa) were 2498 ± 143 (C), 1969 ± 55 (D) and 1832 ± 89 (E) (Ali et al., 2008). On the contrary, the tests completed in this study formed the bulk of those recommended by the standards (International Organization for Standardization, 2013a; International Organization for Standardization, 2013b)and adequate to predict the clinical suitability of the PMMA materials. It is equally justified to assert that they constitute by far the most comprehensive experimental data reported for any 3D printed dental material. Furthermore, the data reported are mostly superior to those reported for milled, 3D-printed, and heat-polymerized denture base materials (Prpić et al., 2020; Fiore et al., 2022; Perea-Lowery et al., 2021).

Conventional acrylic denture base materials have high double bond conversion rate (the percentage of carbon-carbon double bonds converted to single bonds), or degree of conversion (DC) compared to photopolymeric denture base materials. In essence, a material with

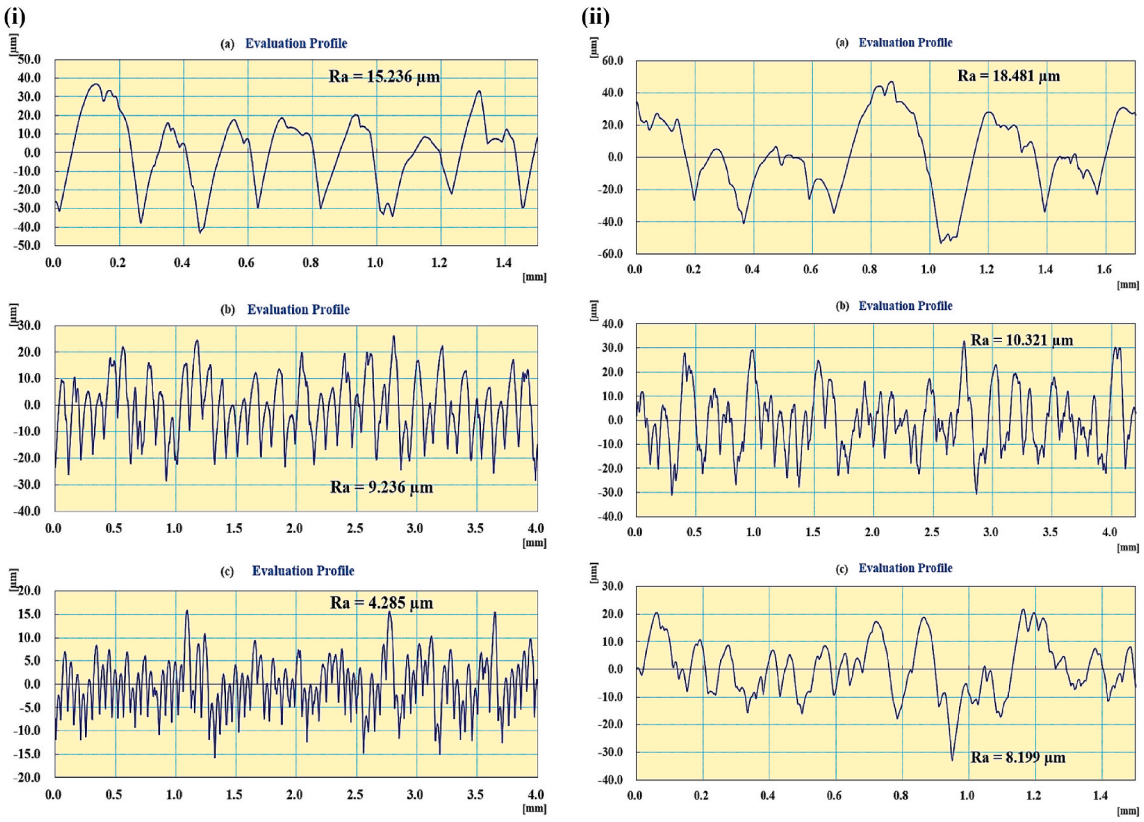

Fig. 22. Ra distribution of (i) pure acrylic versus (ii) 5 vol% fiber reinforced acrylic built at (a) 0.2 mm (b) 0.1 mm (c) 0.05 mm layer heights.

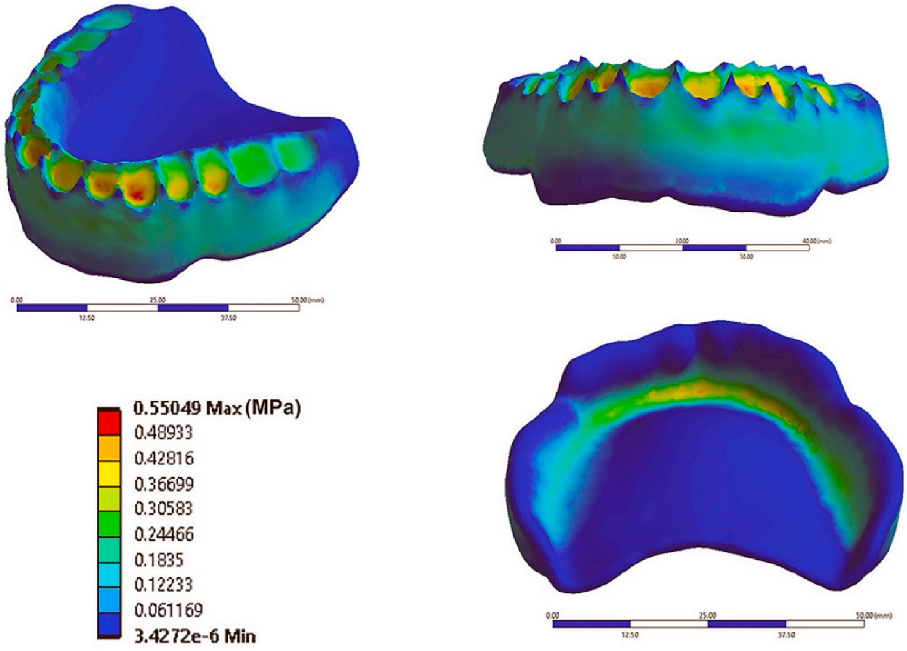

Fig. 23. Finite element analysis of denture bases showing stress distribution, (a) isometric, (b) front, and (c) bottom views.

higher DC may produce superior mechanical properties (strength, hardness, elastic modulus, dimensional stability, solubility, water sorption, and colour stability) and less free monomer that may leach; however, toxicity data on 3D printed denture base photopolymers imply that limited correlation exists between their DC and biological performance (Alifui-Segbaya et al., 2018). The dimethacrylate formulations of the photopolymers are known to exhibit high unsaturated monomers (Alifui-Segbaya et al., 2019b) which may be due to the limited movement of the monomers during onset vitrification of the polymer and the inability of unreacted methacrylate groups to diffuse through the matrix when attached to the polymer (Kim and Watts, 2008).

Esters of acrylic acid have extensive applications in industrial and

Table 6
Homogenized properties of pure (acrylic) polymethylmethacrylate denture bases.

Properties	Homogenized Values	Experimental values	Units	Error %
E_{12}	3.5057	3.644	GPa	3.94%
E_{23}	3.3555	3.356	GPa	0.01%
E_{31}	3.6168	3.429	GPa	5.19%
G_{12}	1.2514		GPa	
G_{23}	1.2376		GPa	
G_{31}	1.2698		GPa	
ν_{12}	0.39466			
ν_{13}	0.38771			
ν_{23}	0.37110			

Key: E – Young's modulus; G - shear modulus; ν - poison ratio.

consumer products (e.g., durable glasslike materials and adhesive materials. Most acrylic acid esters are volatile substances and can produce various clinical symptoms and signs of toxicity if inhaled. In dentistry, the monomers are used to prepare dentures and a variety of filling and coating materials for the teeth (Autian, 1975). Depending on the polymerization type, time, temperature and surface finish and structure, conventional acrylic resins may contain residual methyl methacrylate (MMA) monomers between 0.1% and 5%: 3–5 wt.% in auto-curing PMMA and 0.1–1.5 wt% in heat-polymerizable PMMA.

MMA is an easily flammable substance that may irritate the eyes and respiratory system and may cause acute systemic reactions or embryo-fetal alterations in patients or, after inhalation, in dental personnel or laboratory technicians even if all relevant legal regulations are observed (Geurtsen, 2009). Both MMA and formaldehyde (oxidation product of MMA) can cause local adverse effects such as denture stomatitis (Geurtsen, 2009), systemic toxicity (Geurtsen, 2009; Mir et al., 1973a, 1973b, 1974), cytotoxicity (Gough and Downes, 2001; Kedjarune et al., 1999), skin contact allergies (Brown), burning mouth syndrome (Ali et al., 1985, 1986) and local reactions (Rudigier et al., 1981) depending on the concentration of the residual monomer. The residual MMA contents (0.43% - 0.47%) observed in the materials evaluated are well below the standards threshold (2.2% mass fraction) (International Organization for Standardization, 2013a). The filaments used were fabricated from cross-linked PMMA pellets probably produced by moulding technique hence are likely to contain low residual monomer prior (Alifui-Segbaya et al., 2017) or after processing at an elevated temperature (Geurtsen, 2009). Additionally, the chemical compounds observed in representative PMMA materials in this study are fewer than those observed in photopolymers used for dental devices (Alifui-Segbaya et al., 2020). To reduce residual monomer and degradation products of a dental acrylic, it is recommended that the devices be stored in water up for to 24h in warm water (37–50 °C) before insertion depending on the type of resin and polymerization (Geurtsen, 2009).

Surface roughness (Ra) is a physical property defined as relatively finely spaced surface imperfections whose height, width, and direction establish the predominant surface pattern (Shen et al., 2022). A smooth

Table 8
Experimental parameters used for filament production of PMMA/SGF composites.

Parameters	Type	Values		
Printing direction	(Fixed and categorical)	0° in z-axis	90° in x-y plane	90° in z-axis
Fiber concentration (vol%)	(Random and continuous)	0	2.5	5
Layer height (mm)	(Random and continuous)	0.2	0.1	0.05

Table 7
Chemical compounds identified in acrylic (polymethylmethacrylate) samples.

	Sample 1	MW g/mol	RT [min]	Sample 2	MW g/mol	RT [min]	Sample 3	MW g/mol	RT [min]
Pure PMMA t	2,4-Decadienal	152.23	10.049	2,4-Decadienal	152.23	10.052	2,4-Decadienal	152.23	10.267
	(Z)-2-Decenal	154.25	9.758	(Z)-2-Decenal	154.25	9.759	(Z)-2-Decenal	154.25	9.760
	2-Cyanoacetamide	84.08	1.146	2-Cyanoacetamide	84.08	1.146	2-Cyanoacetamide	84.08	1.146
	Methyl methacrylate	100.12	3.448	Methyl methacrylate	100.12	3.447	Methyl methacrylate	100.12	3.444
	2-Dodecenal	182.30	10.266	2-Dodecenal	182.30	10.266	Hexanal	100.16	5.612
	Nonanal	142.24	8.843	Nonanal	142.24	8.843	2-Tridecenal	196.33	10.267
	Hexanal	100.16	5.610				Heptanal	114.19	7.121
2.5 vol% PMMA/SGF	2-Cyanoacetamide	84.08	1.146	2-Cyanoacetamide	84.08	1.185	2-Cyanoacetamide	84.08	1.154
	Methyl methacrylate	142.24	3.443	Methyl methacrylate	142.24	3.443	Methyl methacrylate	100.12	3.469
	Nonanal	100.12	8.843	Nonanal	100.12	8.856	Nonanal	142.24	8.857
	2-Dodecenal	182.30	10.267	2-Dodecenal	182.30	10.279	Gallic acid iron	226	2.153
	2,4-Decadienal	152.23	10.050	2-Decenal	154.25	9.774			
5 vol% PMMA/SGF	2-Cyanoacetamide	84.08	1.152	2-Cyanoacetamide	1.152	84.08	2-Cyanoacetamide	1.152	1.151
	Methyl methacrylate	100.12	3.467	Methyl methacrylate	3.468	100.12	Methyl methacrylate	3.468	3.467
	Nonanal	142.24	8.857	Nonanal	8.856	142.24	Nonanal	8.856	8.854
	Gallic acid iron	226	2.122	Gallic acid iron	226	2.121			
				2-Decenal	154.25	9.772			

Notes

	Chemical compounds identified in all samples per test batch
T	Chemical compounds identified in 2 of 3 samples per test batch
T	Chemical compound identified in 1 of 3 samples per test batch
T	Chemical compounds identified in all test batches

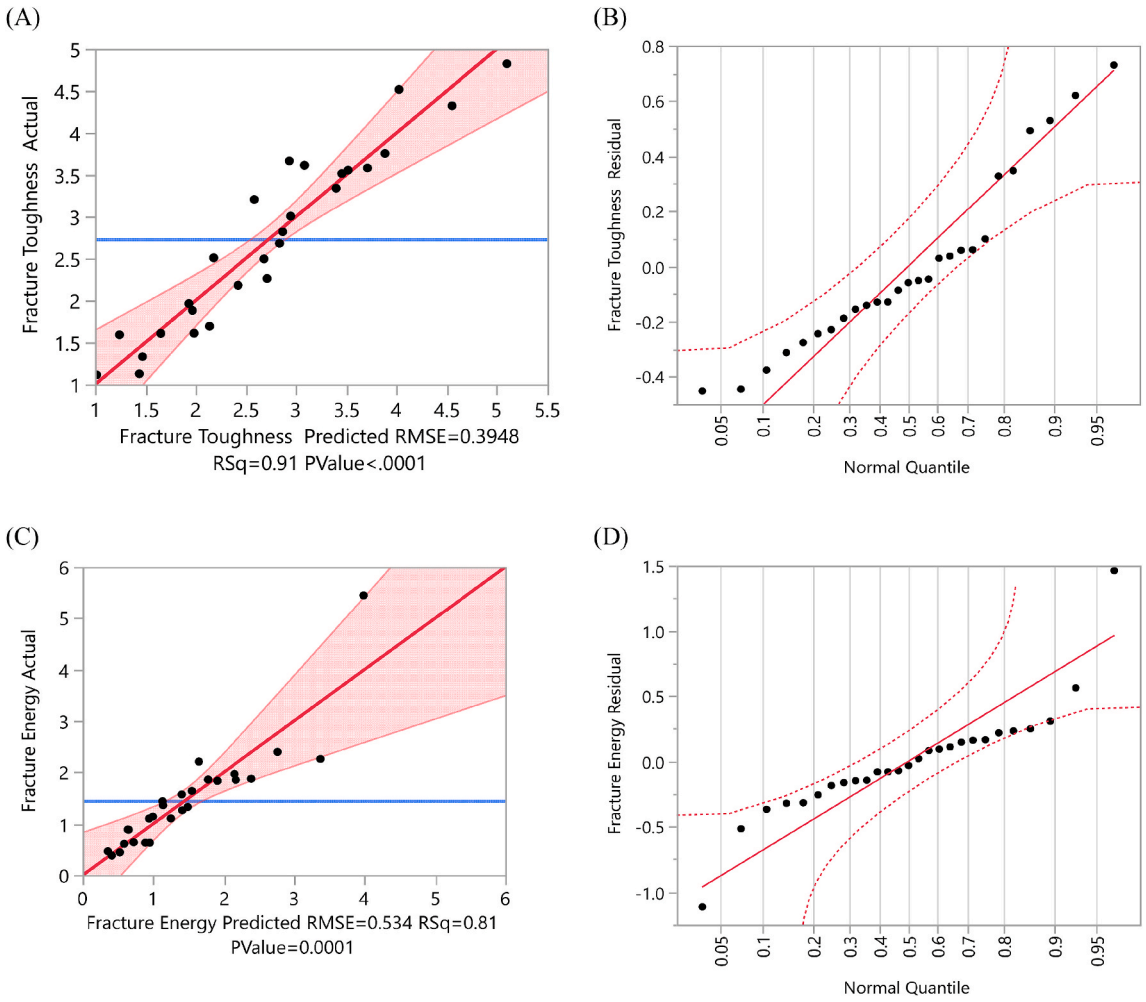

Fig. 24. Plots for residual, predicted and residual normal quantile.

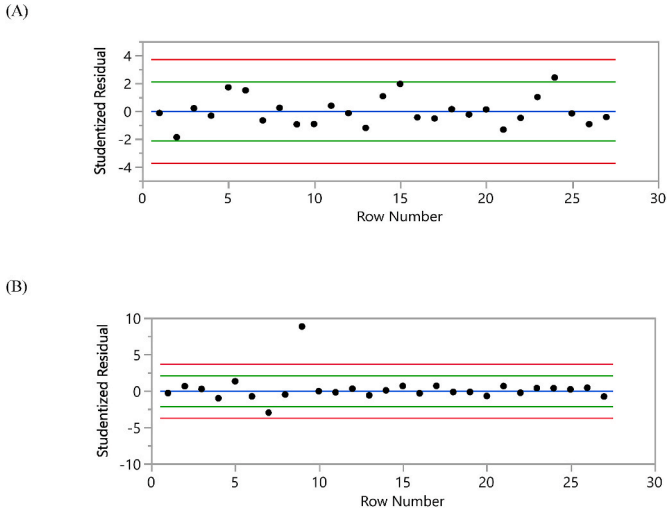

Fig. 25. Plots with variation of residuals for fracture toughness (A) and fracture energy (B).

surface finish (low Ra values) will resist plaque formation or adhesion of microorganisms. Surface roughness value of 0.2 μm has been suggested as the threshold for bacterial retention (Bollen et al., 1997). In determining the mean Ra of denture base materials, studies have recorded

Table 9
ANOVA data from fracture toughness and fracture energy tests.

Variables	DOF	Estimate	Standard error	t ratio	Prob > | t|
For fracture toughness					
Print direction	1	0.861	0.103	8.35	<0.0001
Fiber concentration	1	0.608	0.089	6.81	<0.0001
Layer height	1	-0.531	0.086	-6.12	<0.0001
Two-way interactions					
Print direction: Fiber concentration	1	0.119	0.125	0.96	0.3518
Print direction: Layer height	1	0.062	0.122	0.51	0.6184
Fiber concentration: Layer height		-0.313	0.106	-2.94	0.0091
For fracture energy					
Print direction	1	0.787	0.148	5.31	<0.0001
Fiber concentration	1	0.555	0.128	4.32	0.0005
Layer height	1	-0.363	0.124	-2.91	0.0098
Two-way interactions					
Print direction: Fiber concentration	1	0.309	0.179	1.72	0.1033
Print direction: Layer height	1	-0.196	0.176	-1.11	0.2811
Fiber concentration: Layer height	1	-0.343	0.153	-2.25	0.0383

Table 10
Physical and mechanical properties of acrylic materials vs. standards requirements.

Physical and mechanical properties	Raw PMMA	ISO 20795	Pure PMMA	2.5 vol% PMMA/SGF	5 vol% PMMA/SGF
			0° in z-axis print direction and 0.05 mm layer height		
Flexural strength (MPa)	82 – 117	65 min.	95.92 ± 12.08	126.18 ± 1.60	151 ± 2.30
Flexural modulus (GPa)	2.4 – 3.4	2000 min.	3.08 ± 0.01	3.16 ± 1.60	3.70 ± 0.05
Fracture toughness (MPa $m^{1/2}$)	-	1.9 min.	3.61 ± 0.86	4.81 ± 0.42	4.35 ± 0.66
Fracture work (J/m^2)	-	900 min.	-	-	-
Tensile strength (MPa)	55-75	-	53.85 ± 2.10	66.93 ± 3.30	73.45 ± 2.15
Tensile modulus (GPa)	2.4 – 3.4	-	3.43 ± 0.10	4.48 ± 0.28	4.60 ± 0.22
Compressive strength (MPa)	-	-	77.25 ± 6.06	92.07 ± 2.14	93.16 ± 4.83
Compressive modulus (GPa)	-	-	1.07 ± 0.03	1.35 ± 0.22	1.38 ± 0.08
Thermal conductivity (K)	-	-	0.16	0.16	0.18
Residual MMA (% mass fraction)	-	2.2 max.	0.44	0.43	0.47

different values depending on material type and the processing techniques used. Ra values close to the proposed threshold and <1 μm (Bahrani et al., 2012) or higher (e.g., 3.4–7.61 μm) (Zissis et al., 2000) have been reported for conventional acrylic resins. Similar values close to the threshold (<1 μm) have also been reported for milled, and photopolymers (Gad et al., 2022; Kraemer Fernandez et al., 2020; Al-Dulaijan et al., 2022). The lowest mean Ra values recorded in this study are for materials built in 0° in z-axis with 0.05 mm LH: pure PMMA (5.7 μm), 2.5 vol% PMMA/SGF (6.68 μm) and 5 vol% PMMA/SGF (8.98 μm). Despite the higher values, laboratory finishing, and surface characterization to mimic gingival tissues (Fig. 26) were achieved with ease using crea.lign (Bredent GmbH & Co.KG) permanent veneering composite for polymer substructures.

It is a clinical requirement that "as-built" or "as-processed" denture bases undergo mandatory surface finishing to maximise intraoral function and reduce plaque accumulation (Kuhar and Funduk, 2005). As a rule of thumb, appropriate finishing tools, polishing materials, and handcrafting techniques will be adequate to achieve the desired finish and lustre. In instances where acrylic is considered for dental models, a comparison can be drawn with other materials and techniques as follows: 0.87–4.44 μm for SLA-printed models depending on the build parameters including layer heights; 2.32–2.57 μm for milled polyurethane blanks; 1.72–1.86 μm for Type IV gypsum cast from alginate casting; and 0.98–1.03 μm for Type IV gypsum cast from polyether impression) (Arnold et al., 2019).

4. Conclusion

The strength of this research lies in its novelty as well as the practical implications of the outcomes. The study examined the practicality of the ME process for thermoplastic acrylic (polymethylmethacrylate) intraoral devices and conducted a thorough evaluation of the material and respective composites, against the backdrop of its benefits and recent improvements, current challenges and limitations of photopolymerization-based systems and the inevitability to reconsider their relevance for some applications in dentistry. In many facets, the comprehensive data on physical-mechanical-chemical properties of 3D printed acrylic and acrylic composites is relevant to the contemporary demands of AM in the areas of novel material formulation, characterization, and applications, improved performance, and sustainable approach in the utilization of resources. At a proof-of-concept level, the evidence strengthens the potentials of the processing technology and materials for affordable, lightweight, robust, and safe medical devices. It is envisaged that the findings from this study will generate interests and inform further research towards future adoption and reduce overreliance on established 3DP techniques based on photopolymerization.

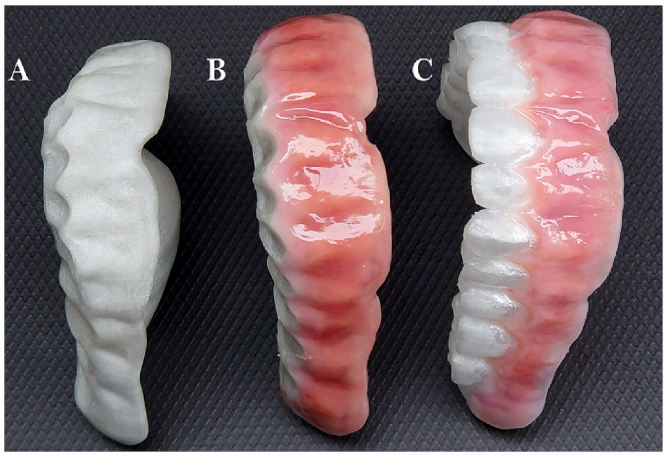

Fig. 26. Laboratory polished denture base prototype (A) and veneered prototypes (B, C). Surface characterization by MDT Nick Georgopoulos.

CRediT authorship contribution statement

Ankit Gupta: Writing – review & editing, Writing – original draft, Visualization, Validation, Methodology, Investigation, Funding acquisition, Formal analysis, Data curation, Conceptualization. **Frank Alifui-Segbaya:** Writing – review & editing, Writing – original draft, Validation, Supervision, Resources, Methodology, Investigation, Funding acquisition, Formal analysis, Data curation, Conceptualization. **Seymur Hasanov:** Writing – review & editing, Writing – original draft, Validation, Data curation, Conceptualization. **Alan R. White:** Validation, Formal analysis. **Khaled E. Ahmed:** Writing – review & editing, Funding acquisition. **Robert M. Love:** Writing – review & editing, Supervision, Funding acquisition. **Ismail Fidan:** Writing – review & editing, Supervision, Resources, Project administration, Methodology, Funding acquisition, Conceptualization.

Declaration of competing interest

The authors declare that they have no known competing financial interests or personal relationships that could have appeared to influence the work reported in this paper.

Data availability

Data will be made available on request.

Acknowledgements

This multidisciplinary collaborative research project between the School of Medicine and Dentistry, Griffith University and Department of Manufacturing and Engineering Technology, Tennessee Technological University, USA was partly funded by The Clark Family Research Award through the Australian Dental Research Foundation (ADRF 2608-2020).

References

Al-Dulaijan, Y.A., Alsulaimi, L., Alotaibi, R., Alboainain, A., Alalawi, H., Alshehri, S., Khan, S.Q., Alsaloum, M., AlRumaih, H.S., Alhumaidan, A.A., Gad, M.M., 2022. Comparative evaluation of surface roughness and hardness of 3D printed resins. Materials 15 (19).

Ali, A., Reynolds, A.J., Bates, J.F., Walker, D.M., 1985. An investigation of the burning mouth sensation related to the wearing of acrylic dentures. J. Dent. Res. 64 (4), 687-687.

Ali, A., Bates, J.F., Reynolds, A.J., Walker, D.M., 1986. The burning mouth sensation related to the wearing of acrylic dentures - an investigation. Br. Dent. J. 161 (12), 444–447.

Ali, I.L., Yunus, N., Abu-Hassan, M.I., 2008. Hardness, flexural strength, and flexural modulus comparisons of three differently cured denture base systems. J. Prosthodont. 17 (7), 545–549.

Alifui-Segbaya, F., 2020. Biomedical photopolymers in 3D printing. Rapid Prototyp. J. 26 (2), 437–444.

Alifui-Segbaya, F., Varma, S., Lieschke, G.J., George, R., 2017. Biocompatibility of photopolymers in 3D printing. 3D Print. Addit. Manuf. 4 (4), 185–191.

Alifui-Segbaya, F., Bowman, J., White, A.R., Varma, S., Lieschke, G.J., George, R., 2018. Toxicological assessment of additively manufactured methacrylates for medical devices in dentistry. Acta Biomater. 78, 64–77.

Alifui-Segbaya, F., Bowman, J., White, A.R., George, R., Fidan, I., 2019a. Characterization of the double bond conversion of acrylic resins for 3D printing of dental prostheses. Compendium of continuing education in dentistry (Jamesburg, N. J. : 1995 40 (10), e7–e11.

Alifui-Segbaya, F., Bowman, J., White, A.R., George, R., Fidan, I., 2019b. Characterization of the double bond conversion of acrylic resins for 3D printing of dental prostheses. Comp. Cont. Educ. Dent. 40 (10) e7–e11.

Alifui-Segbaya, F., Bowman, J., White, A.R., George, R., Fidan, I., Love, R.M., 2020. Chemical characterization of additively manufactured methacrylates for dental devices. Addit. Manuf. 31, 100944.

American Society for Testing and Materials International, 2013. ASTM D 5054 - Standard Test Methods for Plane-Strain Fracture Toughness and Strain Energy Release Rate of Plastic Materials.

American Society for Testing and Materials International, 2014. ASTM E1131-08: Standard Test Method for Compositional Analysis by Thermogravimetry.

American Society for Testing and Materials International, 2016. ASTM D695-15 : Standard Test Method for Compressive Properties of Rigid Plastics.

American Society for Testing and Materials International, 2022. ASTM D638-14: Standard Test Method for Tensile Properties of Plastics.

Arnold, C., Monsees, D., Hey, J., Schweyen, R., 2019. Surface quality of 3D-printed models as a function of various printing parameters. Materials 12 (12), 1970.

Autian, J., 1975. Structure-toxicity relationships of acrylic monomers. Environ. Health Perspect. 11, 141–152.

Bagheri, A., Jin, J., 2019. Photopolymerization in 3D printing. ACS Applied Polymer Materials 1 (4), 593–611.

Bahrani, F., Safari, A., Vojdani, M., Karampoor, G., 2012. Comparison of hardness and surface roughness of two denture bases polymerized by different methods. World J. Dent. 3, 171–175.

Barnett, V., 1975. J. Roy. Stat. Soc. 138 (2), 258-258.

Bollen, C.M., Lambrechts, P., Quirynen, M., 1997. Comparison of surface roughness of oral hard materials to the threshold surface roughness for bacterial plaque retention: a review of the literature. Dent. Mater. 13 (4), 258–269.

D. Brown, Dental materials: biological properties and clinical evaluations, J. Dent. 15(6) 271.

Chua, C.K., Leong, F.K., 2015. 3D Printing and Additive Manufacturing: Principles and Applications, 4 ed. World Scientific Publishing Co. Pte. Ltd., Singapore.

Dizon, J.R.C., Espera, A.H., Chen, Q., Advincula, R.C., 2018. Mechanical characterization of 3D-printed polymers. Addit. Manuf. 20, 44–67.

Fidan, I., Imeri, A., Gupta, A., Hasanov, S., Nasirov, A., Elliott, A., Alifui-Segbaya, F., Nanami, N., 2019. The trends and challenges of fiber reinforced additive manufacturing. Int. J. Adv. Des. Manuf. Technol. 102 (5), 1801–1818.

Fiore, A.D., Meneghello, R., Brun, P., Rosso, S., Gattazzo, A., Stellini, E., Yilmaz, B., 2022. Comparison of the flexural and surface properties of milled, 3D-printed, and heat polymerized PMMA resins for denture bases: an in vitro study. J Prosthodont Res 66 (3), 502–508.

Food and Drug Administration, 2016. Technical Considerations for Additive Manufactured Devices: Draft Guidance for Industry and Food and Drug Administration Staff. Food and Drug Administration, Rockville (MD).

Gad, M., Rahoma, A., Abualsaud, R., Ammar, M., 2018. Tensile strength of denture base material reinforced with zirconia nanoparticle and glass fibers. Al-Azhar Dental Journal for Girls 5 (3), 285–295.

Gad, M.M., Fouda, S.M., Abualsaud, R., Alshahrani, F.A., Al-Thobity, A.M., Khan, S.Q., Akhtar, S., Ateeq, I.S., Helal, M.A., Al-Harbi, F.A., 2022. Strength and surface properties of a 3D-printed denture base polymer. J. Prosthodont. 31 (5), 412–418.

Geurtsen, W., 2009. Polymethylmethacrylate Resins, Biocompatibility of Dental Materials. Springer Berlin Heidelberg, Berlin, Heidelberg, pp. 255–270.

Gough, J.E., Downes, S., 2001. Osteoblast cell death on methacrylate polymers involves apoptosis. J. Biomed. Mater. Res. 57 (4), 497–505.

Gupta, A., Fidan, I., Hasanov, S., Nasirov, A., 2020. Processing, mechanical characterization, and micrography of 3D-printed short carbon fiber reinforced polycarbonate polymer matrix composite material. Int. J. Adv. Des. Manuf. Technol. 107 (7), 3185–3205.

Gupta, A., Hasanov, S., Fidan, I., Zhang, Z., 2022. Homogenized modeling approach for effective property prediction of 3D-printed short fibers reinforced polymer matrix composite material. Int. J. Adv. Des. Manuf. Technol. 118 (11), 4161–4178.

Hasanov, S., 2021. Numerical Modeling and Experimental Characterization of Functionally Graded Materials Manufactured by the Fused Filament Fabrication Process. Tennessee Technological University.

Hasanov, S., Gupta, A., Alifui-Segbaya, F., Fidan, I., 2021. Hierarchical homogenization and experimental evaluation of functionally graded materials manufactured by the fused filament fabrication process. Compos. Struct. 275, 114488.

Hasanov, S., Alkunte, S., Rajeshirke, M., Gupta, A., Huseynov, O., Fidan, I., Alifui-Segbaya, F., Rennie, A., 2022. Review on additive manufacturing of multi-material parts: progress and challenges. Journal of Manufacturing and Materials Processing 6 (1), 4.

International Organization for Standardization, 2013a. ISO 20795-1, Dentistry - Base Polymers - Part 1: Denture Base Polymers. International Organization for Standardization, Geneva.

International Organization for Standardization, 2013b. ISO 20795-2, Dentistry-Base Polymers - Part 2: Orthodontic Base Polymers. International Organization for Standardization, Geneva.

International Organization for Standardization, 2019. ISO 178:2019 Plastics — Determination of Flexural Properties.

Jancar, J., Hynstova, K., Pavelka, V., 2009. Toughening of denture base resin with short deformable fibers. Compos. Sci. Technol. 69 (3), 457–462.

John, J., Gangadhar, S.A., Shah, I., 2001. Flexural strength of heat-polymerized polymethyl methacrylate denture resin reinforced with glass, aramid, or nylon fibers. J. Prosthet. Dent 86 (4), 424–427.

Kedjarune, U., Charoenworaluk, N., Koontongkaew, S., 1999. Release of methyl methacrylate from heat-curved and autopolymerized resins: cytotoxicity testing related to residual monomer. Aust. Dent. J. 44 (1), 25–30.

Kim, S.-H., Watts, D.C., 2008. Degree of conversion of bis-acrylic based provisional crown and fixed partial denture materials. The Journal of Korean Academy of Prosthodontics 46 (6), 639–643.

Kraemer Fernandez, P., Unkovskiy, A., Benkendorff, V., Klink, A., Spintzyk, S., 2020. Surface characteristics of milled and 3D printed denture base materials following polishing and coating: an in-vitro study. Materials 13 (15), 3305.

Kuhar, M., Funduk, N., 2005. Effects of polishing techniques on the surface roughness of acrylic denture base resins. J. Prosthet. Dent 93 (1), 76–85.

Kul, E., Aladağ, L.İ., Yesildal, R., 2016. Evaluation of thermal conductivity and flexural strength properties of poly(methyl methacrylate) denture base material reinforced with different fillers. J. Prosthet. Dent 116 (5), 803–810.

Lawrence, E.. ASTM D638: the definitive guide to plastic tensile testing. https://www.instron.com/en/testing-solutions/astm-standards/astm-d638. 2023.

Ligon, S.C., Liska, R., Stampfl, J., Gurr, M., Mülhaupt, R., 2017. Polymers for 3D printing and customized additive manufacturing. Chem. Rev. 117 (15), 10212–10290.

Liu, T., Tian, X., Zhang, M., Abliz, D., Li, D., Ziegmann, G., 2018. Interfacial performance and fracture patterns of 3D printed continuous carbon fiber with sizing reinforced PA6 composites. Compos. Appl. Sci. Manuf. 114, 368–376.

Lourinho, C., Salgado, H., Correia, A., Fonseca, P., 2022. Mechanical properties of polymethyl methacrylate as denture base material: heat-polymerized vs. 3D-printed—systematic review and meta-analysis of in vitro studies. Biomedicines 10 (10), 2565.

Lüchtenborg, J., Burkhardt, F., Nold, J., Rothlauf, S., Wesemann, C., Pieralli, S., Wemken, G., Witkowski, S., Spies, B.C., 2021. Implementation of fused filament fabrication in dentistry. Appl. Sci. 11 (14), 6444.

Mazumdar, P., Chowdhury, D., 2021. Manual of Laboratory Testing Methods for Dental Restorative Materials. John Wiley & Sons, Inc., Hoboken, NJ.

Mir, G.N., Lawrence, W.H., Autian, J., 1973a. Toxicological and pharmacological actions of methacrylate monomers I: effects on isolated, perfused rabbit heart. J. Pharmaceut. Sci. 62 (5), 778–782.

Mir, G.N., Lawrence, W.H., Autian, J., 1973b. Toxicological and pharmacological actions of methacrylate monomers II: effects on isolated Guinea pig ileum. J. Pharmaceut. Sci. 62 (8), 1258–1261.

Mir, G.N., Lawrence, W.H., Autian, J., 1974. Toxicological and pharmacological actions of methacrylate monomers III: effects on respiratory and cardiovascular functions of anesthetized dogs. J. Pharmaceut. Sci. 63 (3), 376–381.

Nasirov, A., Gupta, A., Hasanov, S., Fidan, I., 2020. Three-scale asymptotic homogenization of short fiber reinforced additively manufactured polymer composites. Compos. B Eng. 202, 108269.

Nathan-Walleser, T., Lazar, I.-M., Fabritius, M., Tölle, F.J., Xia, Q., Bruchmann, B., Venkataraman, S.S., Schwab, M.G., Mülhaupt, R., 2014. 3D micro-extrusion of graphene-based active electrodes: towards high-rate AC line filtering performance electrochemical capacitors. Adv. Funct. Mater. 24 (29), 4706–4716.

Nejatian, T., Pezeshki, S., Yaqin Syed, A.U., 2019. 5 - acrylic denture base materials. In: Khurshid, Z., Najeeb, S., Zafar, M.S., Sefat, F. (Eds.), Advanced Dental Biomaterials. Woodhead Publishing, pp. 79–104.

Perea-Lowery, L., Gibreel, M., Vallittu, P.K., Lassila, L.V., 2021. 3D-Printed vs. Heat-polymerizing and autopolymerizing denture base acrylic resins. Materials 14 (19), 5781.

Pieralli, S., Spies, B.C., Hromadnik, V., Nicic, R., Beuer, F., Wesemann, C., 2020. How accurate is oral implant installation using surgical guides printed from a degradable and steam-sterilized biopolymer? J. Clin. Med. 9 (8), 2322.

Prpić, V., Schauperl, Z., Ćatić, A., Dulčić, N., Čimić, S., 2020. Comparison of mechanical properties of 3D-printed, CAD/CAM, and conventional denture base materials. J. Prosthodont. 29 (6), 524–528.

Rajisha, K.R., Deepa, B., Pothan, L.A., Thomas, S., 2011. 9 - thermomechanical and spectroscopic characterization of natural fibre composites. In: Zafeiropoulos, N.E.

(Ed.), Interface Engineering of Natural Fibre Composites for Maximum Performance. Woodhead Publishing, pp. 241–274.
Rudigier, J., Scheuermann, H., Kotterbach, B., Ritter, G., 1981. [Release and diffusion of methylmethacrylic monomers after the implantation of self curing bone cements. Study on laboratory specimens and animal experiments (author's transl)]. Unfallchirurgie 7 (3), 132–137.
Sakaguchi, R.L., 2012. Chapter 9 - restorative materials: composites and polymers. In: Powers, J.M. (Ed.), Craig's Restorative Dental Materials, thirteenth ed. Mosby, Saint Louis, pp. 161–198.
Sharafi, S., Santare, M.H., Gerdes, J., Advani, S.G., 2021. A review of factors that influence the fracture toughness of extrusion-based additively manufactured polymer and polymer composites. Addit. Manuf. 38, 101830.
Shen, C., Rawls, H.R., Esquivel-Upshaw, J.F., 2022. Phillips' Science of Dental Materials. Elsevier, St. Louis, Missouri.
Sideridou, I.D., 2010. Polymeric Materials in Dentistry. Nova Science Publishers, Inc, New York.
Stansbury, J.W., Idacavage, M.J., 2016. 3D printing with polymers: challenges among expanding options and opportunities. Dent. Mater. 32 (1), 54–64.
Terekhina, S., Tarasova, T., Egorov, S., Skornyakov, I., Guillaumat, L., Hattali, M.L., 2020. The effect of build orientation on both flexural quasi-static and fatigue behaviours of filament deposited PA6 polymer. Int. J. Fatig. 140, 105825.
Tian, X., Liu, T., Yang, C., Wang, Q., Li, D., 2016. Interface and performance of 3D printed continuous carbon fiber reinforced PLA composites. Compos. Appl. Sci. Manuf. 88, 198–205.
Tran, T.Q., Ng, F.L., Kai, J.T.Y., Feih, S., Nai, M.L.S., 2022. Tensile strength enhancement of fused filament fabrication printed parts: a review of process improvement approaches and respective impact. Addit. Manuf. 54, 102724.
Vaidya, A., Pathak, K., 2019. 17 - mechanical stability of dental materials. In: Asiri, A.M., Inamuddin, Mohammad, A. (Eds.), Applications of Nanocomposite Materials in Dentistry. Woodhead Publishing, pp. 285–305.
van Noort, R., 2012. The future of dental devices is digital. Dent. Mater. 28 (1), 3–12.
Väyrynen, V.O.E., Tanner, J., Vallittu, P.K., 2016. The anisotropicity of the flexural properties of an occlusal device material processed by stereolithography. J. Prosthet. Dent 116 (5), 811–817.
Ventola, C.L., 2014. Medical applications for 3D printing: current and projected uses. P T 39 (10), 704–711.
Zissis, A.J., Polyzois, G.L., Yannikakis, S.A., Harrison, A., 2000. Roughness of denture materials: a comparative study. Int. J. Prosthodont. (IJP) 13 (2), 136–140.